chemosensors

Review

Review on Anti-Aggregation-Enabled Colorimetric Sensing Applications of Gold and Silver Nanoparticles

Muthaiah Shellaiah and Kien-Wen Sun *

Department of Applied Chemistry, National Yang Ming Chiao Tung University, Hsinchu 300, Taiwan
* Correspondence: kwsun@nycu.edu.tw

Abstract: Gold- and silver nanoparticles (Au NPs and Ag NPs)-based colorimetric detection of specific analytes has attracted intense research interest and is still in great demand. The majority of Au NPs- and Ag NPs-based sensory reports have revealed that, during the analyte recognition, dispersed NPs typically aggregated and displayed color changes from wine-red to blue/purple and yellow to orange/brown, respectively. On the other hand, only a few reports demonstrated that the aggregated Au NPs and Ag NPs underwent anti-aggregation in the presence of certain analytes, which displayed reversed color changes from blue/purple to wine-red and orange/brown to yellow, correspondingly. There are some examples of anti-aggregation phenomena mentioned in a vast number of studies on Au NPs- and Ag NPs-based colorimetric sensors via NP aggregation. However, a review targeting the anti-aggregation-enabled Au NPs- and Ag NPs-based colorimetric sensing of diverse analytes is not yet available. In this review, anti-aggregation-facilitated Au NPs- and Ag NPs-based colorimetric detection of metal ions, anions, bio-analytes, pesticides, and herbicides is delivered with detailed underlying mechanisms. Moreover, the probe design, sensory requirement, merits, limitations, and future scope of anti-aggregation-enabled Au NPs- and Ag NPs-based colorimetric sensors are discussed.

Keywords: ion detection; aggregation; anti-aggregation; Au NPs; Ag NPs; colorimetric recognition; real analysis; biosensors; pesticides; herbicides

Citation: Shellaiah, M.; Sun, K.-W. Review on Anti-Aggregation-Enabled Colorimetric Sensing Applications of Gold and Silver Nanoparticles. *Chemosensors* **2022**, *10*, 536. https://doi.org/10.3390/chemosensors10120536

Academic Editor: Christos Kokkinos

Received: 19 October 2022
Accepted: 13 December 2022
Published: 16 December 2022

1. Introduction

To sustain the eco-systems, detection and quantification of biological and environmental contaminants, such as metal ions, anions, bio-analytes, pesticides, and herbicides, are essential [1–5]. Thus, several tactics have been employed for analytes/hazards detection, including nanoprobes-based colorimetric/fluorometric assay, instrumentation-based quantification, metal-organic frameworks (MOFs)-tuned analyte detection, and organic/polymeric probes-based sensors, etc. [6–15]. Among them, the luminescent probes are the top performers in terms of their real-time bioimaging applications [16–20]. Likewise, the gold- and silver nanoparticles (Au NPs and Ag NPs)-based colorimetric assay of biological and environmental contaminants is attested to be effective in real water interrogations [21–25]. In the presence of a specific analyte, the Au NPs and Ag NPs displayed a color change from wine-red to blue/purple and yellow to orange/brown, respectively [26–30]. In these sensory investigations, the color change was attributed to the analyte-induced aggregation of dispersed Au NPs and Ag NPs [31].

In contrast, specific analytes can induce the anti-aggregation to reverse the origin color of Au NPs and Ag NPs from blue/purple to wine-red and orange/brown to yellow, correspondingly [32,33]. In fact, other than NPs-based colorimetric sensors, anti-aggregation is also a property possessed by many nanomaterials, such as selenium nanoparticles (Se NPs), cerium oxide (CeO_2), copper nanoparticles (Cu NPs), and molybdenum disulfide nanosheets (MoS_2 NS) and has been applied in amyloid-beta inhibition, reactive oxygen

species (ROS) generation, disease treatment, etc. [34–38]. To achieve anti-aggregation-induced colorimetric responses, both aggregated Au NPs and Ag NPs must interact with specific aggregation-inducing agents or reactive analyte sensing units, which have a high sensitivity for specific analytes and can be released from the NPs' surface [39]. In the presence of specific analytes, aggregation-inducing agents can be replaced by electrostatic interactions, disturbance of coordinative binding, oxidation/reduction of aggregation-inducing agents, and coordinative complexation with analyte, thereby re-dispersing the Au NPs/Ag NPs and reversing the color changes [32–39].

Highly concentrated toxic/heavy metal ions, anions, bio-analytes, pesticides, and herbicides significantly affect the eco-system [40–45]. Researchers developed numerous tactics including the anti-aggregation strategy to overcome contaminations caused by the above toxic/hazard species [6–33]. Recently, a review paper discussing the use of anti-aggregation of Au NPs for metal ions detection was reported by Najafzadeh et al. [46]. However, a thorough review on the anti-aggregation of Au NPs/Ag NPs for discriminating anions, bio-analytes, pesticides, herbicides, and metal ions detection is not yet available, which motivates us to write this review.

In this review, utilization of the anti-aggregation strategy in the Au NPs/Ag NPs-based colorimetric detection of metal ions, anions, bio-analytes, pesticides, and herbicides is illustrated with mechanistic and binding details. Uniqueness of its design, linear range, limit of detection (LOD), and real-time applicability are discussed with future scopes. The schematic shown in Figure 1 illustrates the anti-aggregation strategy applied in Au NPs/Ag NPs-based colorimetric sensors toward metal ions, anions, bio-analytes, pesticides, and herbicides.

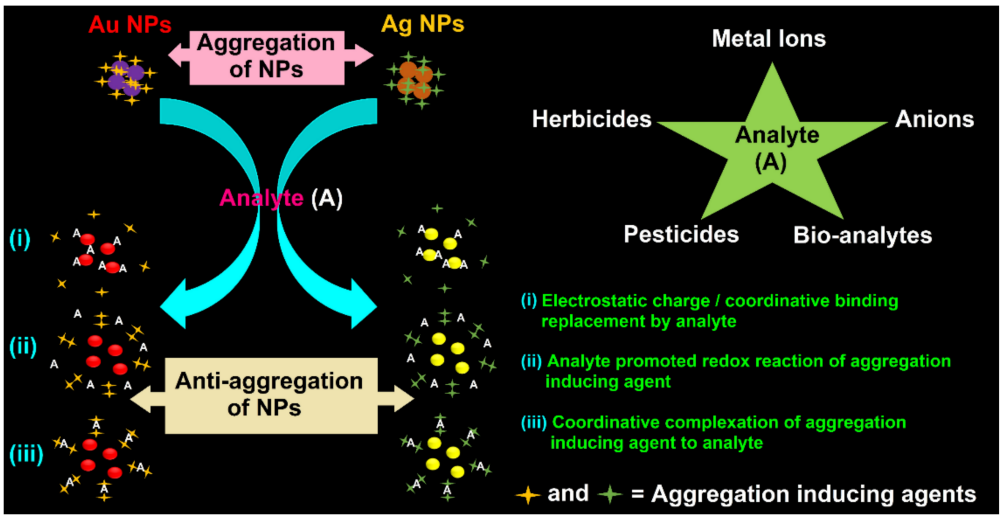

Figure 1. Schematic of the anti-aggregation strategy applied in Au NPs/Ag NPs-based colorimetric sensors toward metal ions, anions, bio-analytes, pesticides, and herbicides.

2. Au NPs-Based Colorimetric Assay of Metal Ions via Anti-Aggregation

In regard to the anti-aggregation-enabled Au NPs-based colorimetric metal ions detection, quantification of Hg^{2+} has attracted much attention by numerous researchers [47–57]. Li and co-workers described the use of label-free citrate–capped Au NPs (CI-Au NPs; particle size = 13 nm; (nm = nanometer)) as a colorimetric probe toward mercury ions detection via the anti-aggregation strategy [47]. In this work, the 4,4′-dipyridyl (DPy; 5.2 μM (μM = micromole)) acted as an aggregation-inducing agent of Au NPs that can be released from the NPs' surface because of its exceptional coordination ability toward Hg^{2+}. When the 4,4′-dipyridyl induces Au NPs aggregation, the color changes from red to blue. However, in the presence of Hg^{2+}, it changes back to its original red color due to anti-aggregation, as represented in Figure 2A. None of the metal ions, except Hg^{2+}, displays colorimetric reversibility as seen in Figure 2B. The best result was obtained at

pH 7 (buffer: 10 mM Tris(hydroxymethyl)aminomethane hydrochloride (Tris-HCl)) after 30 min incubation (min = minutes). Transmission electron microscopy (TEM) studies clearly attested the anti-aggregation of Au NPs. Surface plasmon resonance (SPR at A_{520}/A_{620}) studies revealed the linearity to be between 0.04 and 1.1 µM, with an estimated limit of detection (LOD) of 15 nM (nM = nanomole). This work was also demonstrated with tap water and spring water samples (with 100-fold excess interference ions) investigations; therefore, it can be utilized for Hg^{2+} quantification in real time.

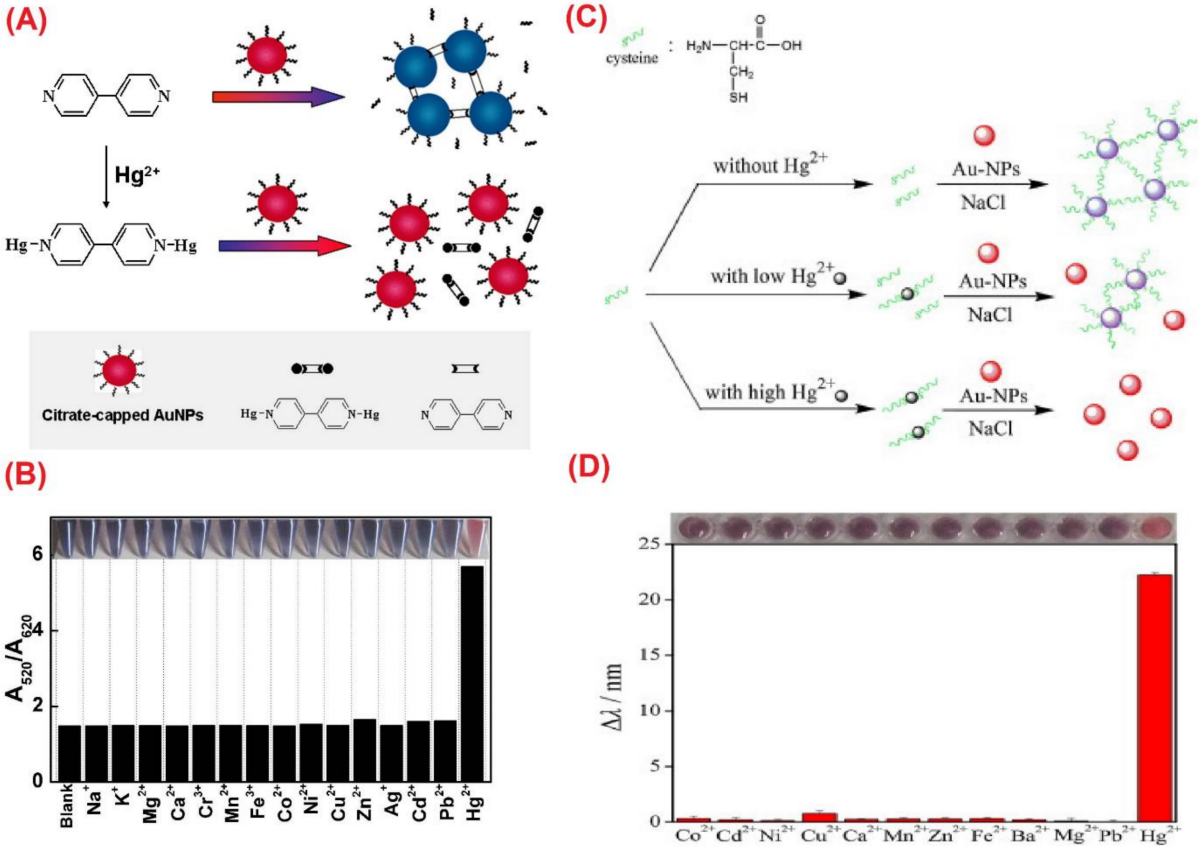

Figure 2. (**A**) Schematic representation of anti-aggregation of Au NPs for the detection of Hg^{2+}; (**B**) absorbance ratio of A_{520}/A_{620} and photographic images (inset) of solutions containing Au NPs, DPy (4,4′-Dipyridine; 2.5 µM), and various metal ions (each 100 µM, except Hg^{2+} 1.0 µM) ((**A**,**B**) are reproduced with the permission from [47]); (**C**) schematic illustration of the determination of Hg^{2+} by PDDA-Au NPs in the presence of Cys; (**D**) the SPR band shift relative to Cys-Au NPs (Δλ) and photographic image of Au NPs solutions containing 0.7 µg/mL Cys, 1.0×10^{-4} M EDTA-Na_2, and 1.0×10^{-5} M various metal ions. ((**C**,**D**) are reproduced with the permission from [48]).

Following a similar approach, Ding et al. described anti-aggregation-mediated colorimetric detection of Hg^{2+} by dislocating the aggregation-inducing agent cysteine (Cys; 7 µg/mL) at 0.1 M NaCl [48]. In the study, positively charged Au NPs were synthesized using poly(diallyldimethylammonium) chloride (PDDA) to afford PDDA-Au NPs (particle size = 12.2 nm). The PDDA acted as a reducer and stabilizer at the same time. Adding the Cys into PDDA-Au NPs led to a color change from ruby red to royal purple via aggregation. In the early stage, the aggregation was negligible due to the strong electrostatic repulsion between PDDA-Au NPs and Cys. However, after adding 0.1 M of NaCl, the electrostatic repulsion became weaker, and the Cys-Au NPs aggregates were formed. A pH value of 5 (Buffer: acetic acid–sodium acetate (HAc-NaAc)) was selected to enhance the strong Au-S binding (via zwitterionic Cys form) in the Cys-Au NPs aggregates. Owing to the strong interaction between Cys and Hg^{2+}, it was more favorable for the Hg-Cys complex formation; therefore, it prevented the Cys-Au NPs aggregates and reversed the

color back to ruby red. This anti-aggregation behavior was demonstrated by TEM and SPR (at A_{520}/A_{610}) studies. Among other metallic species, Pb^{2+} and Cu^{2+} also displayed a certain degree of anti-aggregation by forming a complex with Cys, which can be avoided by using the masking agent EDTA-Na_2 (ethylenediaminetetraacetic acid disodium salt). Figure 2C,D demonstrate the anti-aggregation of the Au NPs-Cys system in the presence of Hg^{2+}. The Hg^{2+} shows the linear range to be between 0.05 and 10 μM with an LOD of 25 nM. This work was demonstrated in drinking water samples (>100% recovery), but more interrogations are required to further understand the underlying mechanism.

Aggregation of citrate-capped (CI) Au NPs (particle size = 13 nm; conc. = 15 nM (conc. = concentration)) was induced by thymine via citrate replacement from the NPs' surface. When Hg^{2+} was present, it interacted with thymine to afford anti-aggregation-enabled reversibility of the original SPR and color [49]. In the presence of thymine (0.2 mM), the color of CI-Au NPs turned to blue. When Hg^{2+} was added, a "thymine-Hg^{2+}-thymine" motif was formed, which released the thymine from the Au NPs' surface and reversed the color back to the original red through the anti-aggregation (see the TEM and SPR (at A_{520}/A_{670}) interrogations). Optimum pH condition and incubation time were established as pH 8 (buffer: 1 mM Tris-HCl) and 30 min. None of the ions, except the Hg^{2+}, induced anti-aggregation and exhibited significant recoveries (88–112.5%) in tap water samples. This report can be regarded as a novel work in terms of its uncomplicated procedure, linearity (2–12 μM), LOD (2 nM), and real-time applicability. Subsequently, O-phenylenediamine (OPD; 3.1 μM) induced CI-Au NPs aggregations (particle size = 7–11 nm) and displayed a color change from red to blue [50]. By adding Hg^{2+} to the OPD-Au NPs complex system, the anti-aggregation was initiated via OPD-Hg^{2+} complexes formation (after 20 min incubation time), and the color was changed back from blue to red. The effective coordination between Hg^{2+} and OPD is directed by two amine (-NH_2) groups present in OPD at an operative pH value of 6.5. As seen in Figure 3A,B, none of the metal ions, except Hg^{2+}, shows high selectivity via anti-aggregation. This was also confirmed by TEM, SPR (at A_{520}/A_{680}), and density functional theory (DFT) investigations as well. The linear regression of Hg^{2+} was between 0.01 and 2 μM, with an LOD of 5 nM. This work was applied to tap water and lake water samples interrogations, which showed recoveries of between 70 and 120%. In terms of its high colorimetric selectivity, linear range, LOD, theoretical support, and real sample studies, this report can be regarded as a unique work in Hg^{2+} quantification.

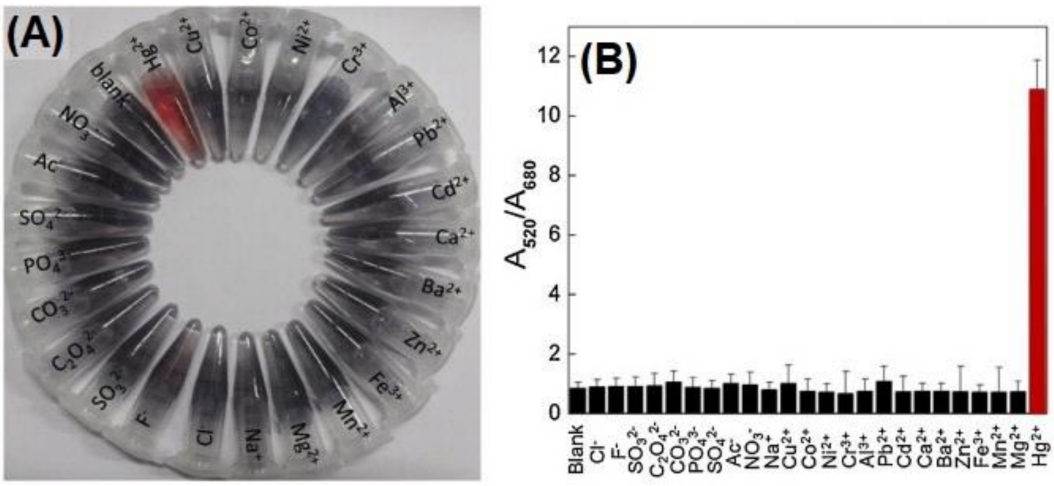

Figure 3. Selectivity of the Au NPs-based detection system (containing 3.1 μM of OPD) for Hg^{2+} compared with other ions. (**A**) Photograph of the detection systems incubated with Hg^{2+} (2.0 μM) or other ions (20 μM); (**B**) A_{520}/A_{680} (ratio of the absorbance value at 520 nm to that at 680 nm in the UV–vis spectra) of the detection systems incubated with Hg^{2+} (2.0 μM) or other ions (20 μM) (mean ± SD, n = 3) ((**A**,**B**) are reproduced with the permission from [50]).

The CI-Au NPs were engaged in anti-aggregation-enabled colorimetric detection of Hg^{2+} as described by the following: The L-penicillamine (Pen; optimum concentration fixed as 3.5 μM) induced aggregation of CI-Au NPs (particle size = 20 nm; conc. = 2.85 nM) as evident from the emerging of a new absorbance peak at 750 nm. The absorption peak was blue-shifted to 525 nm due to anti-aggregation and effective binding of penicillamine to Hg^{2+} (via Pen-Hg^{2+}-Pen complex) when Hg^{2+} was added [51]. Both aggregation and anti-aggregation were attested by TEM studies. Detection of Hg^{2+} showed the linearity as being between 50 and 400 nM (at A_{525}/A_{750}), with an LOD of 25 nM. This work was supported by spiked tap water investigations, but the appropriate pH for this sensor was predicted to be acidic pH 2.4 (buffer: 5 mM citric acid–sodium citrate), thereby requiring more clarifications on its reliability. Zhou et al. utilized the 4-mercaptophenylboronic acid (MPBA; 10 μM) as an aggregation-inducing agent with CI-Au NPs (particle size = 15 nm) for colorimetric detection of Hg^{2+} by means of anti-aggregation [52]. The citrate attached on the NP surface was replaced by MPBA (via Au-S bond) and led to aggregation, thereby changing the color from red to blue.

When Hg^{2+} is present, the MPBA coordinates with Hg^{2+} via strong Hg-S interactions to initiate the anti-aggregation accompanied with a color change from blue to red as demonstrated in Figure 4A. The best result was attained at pH 4 (buffer: 10 mM citric acid–sodium citrate) after 20 min incubation.

Detection of Hg^{2+} shows colorimetric response and linear regression as being between 0.01 and 5 μM (at A_{520}/A_{690}), with an LOD of 8 nM, as seen in Figure 4C,D. TEM studies confirmed the anti-aggregation in the Hg^{2+} detection, and none of the other metal ions displayed the interfering effect. Moreover, spiked lake water interrogations showed recoveries of between 96.3 and 110%, thereby approving its real-time applicability. In a similar fashion, free thiol (-SH) containing aggregation-inducing agents, such as N-Acetyl-L-cysteine (NAC; 10 μM; 30 min incubation time; pH 7 (buffer: phosphate buffer saline (PBS) prepared from NaH_2PO_4 and Na_2HPO_4)) and 2-Mercapto-benzothiazole (MBT; 2.2 μM; 5 min incubation time; pH 5.8 (buffer: PBS)), were used in discrimination of Hg^{2+} [53,54]. Both agents induced aggregation of CI-Au NPs (particle size = 15 nm (conc. = 15 nM) and 10–20 nm, respectively) and observed a color change from red to blue, which was then disrupted by Hg^{2+}-enabled anti-aggregation with a reversed color change from blue to red. The dimeric complexes (NAC-Hg-NAC and MBT-Hg-MBT) were formed with those reactive agents because of the high binding tendency of Hg to S. The linear regression of Hg^{2+} was reported to have values between 0.02 and 1 μM (at A_{520}/A_{620}) and 0.05–1 μM (at A_{700}/A_{520}), with calculated LODs of 9.9 nM and 6 nM, respectively. Both reports were well authorized by TEM and recovery studies in real water and milk samples analysis; therefore, they can be regarded as notable reports in anti-aggregation-mediated Hg^{2+} quantification.

Rajeshwari and co-workers proposed a tween 20-modified gold nanorods (Au NRs; average length = 45.11 ± 0.64 nm and diameter = 17.95 ± 0.38 nm)-based detection of Hg^{2+} via the anti-aggregation strategy [55]. Herein, dithiothreitol (DTT; 1.5 μM) firstly induced aggregation of NRs. When Hg^{2+} was added, the strong binding affinity of DTT to Hg^{2+} turned the aggregations into dispersed NRs. The linear regression of Hg^{2+} was between 1 and 100 pM (SPR at 679 nm; pH 7.4 (buffer: Tris-HCl); pM = picomole), with an LOD of 0.42 pM. This work also conducted studies in stimulated body fluid recovery, but they lacked colorimetric responses. Sun et al. utilized the hexadecyl trimethyl ammonium bromide (CTAB; 0.44 μM) to induce aggregation of CI-Au NPs (particle size = 13 nm; conc. = 8.7 nM), which was dis-aggregated by Hg^{2+} via anti-aggregation with a corresponding color change from blue to red [56]. The best pH and response time were determined to be pH 7 (buffer: Tris-HCl) and 30 min. In the beginning, aggregation of NPs took place due to strong electrostatic attraction between CI-Au NPs and CTAB, with a respective color change from red to blue. In the presence of Hg^{2+}, Au NPs tend to form a Hg-Au alloy, which hinders the electrostatic attraction and inhibits aggregation caused by CTAB, as shown in Figure 5A. The linear range of Hg^{2+} was between 0 and 0.68 μM (at A_{650}/A_{520}), with an LOD of 11.9 nM. The anti-aggregation was confirmed and attested by TEM and

DLS (DLS = dynamic light scattering) investigations and by tap water recovery (>90%; RSD $\leq$ 4% (RSD = relative standard deviation)). Therefore, it can be regarded as an important probe toward Hg^{2+} quantitation. Thereafter, 3, 5-Dimethyl-1-thiocarboxamidepyrazole (Pzl; 1.5 µM)-induced aggregation of CI-Au NPs (particle size = 14 nm; conc. = 15 nM) was utilized for the colorimetric detection of Hg^{2+} [57]. In the presence of Pzl, the color of the CI-Au NPs changed from red to blue via aggregation, which was reversed (from blue to red) in the presence of Hg^{2+} by means of anti-aggregation. The reason of the color reverse to the original (as shown in Figure 5B) is that the Pzl goes through coordination with Hg^{2+} to form a Pzl-Hg-Pzl complex due to the presence of the functional unit -C = S. None of the ions, except Hg^{2+}, displayed interfering selectivity. The optimum response was found at pH 5.6–8 (buffer: PBS) after 3–4 min incubation. The anti-aggregation mechanism and dimeric mercury complex of Pzl were clarified and confirmed by TEM studies and DFT optimization, respectively. The linearity of Hg^{2+} was between 0.01 and 1.5 µM (at A_{680}/A_{520}), with an LOD of 7.7 nM, and was attested by recovery studies in tap water and lake water (lies between 94 and 105%). Based on the TEM, DLS, and real samples analysis, this report can be regarded as a well accomplished work.

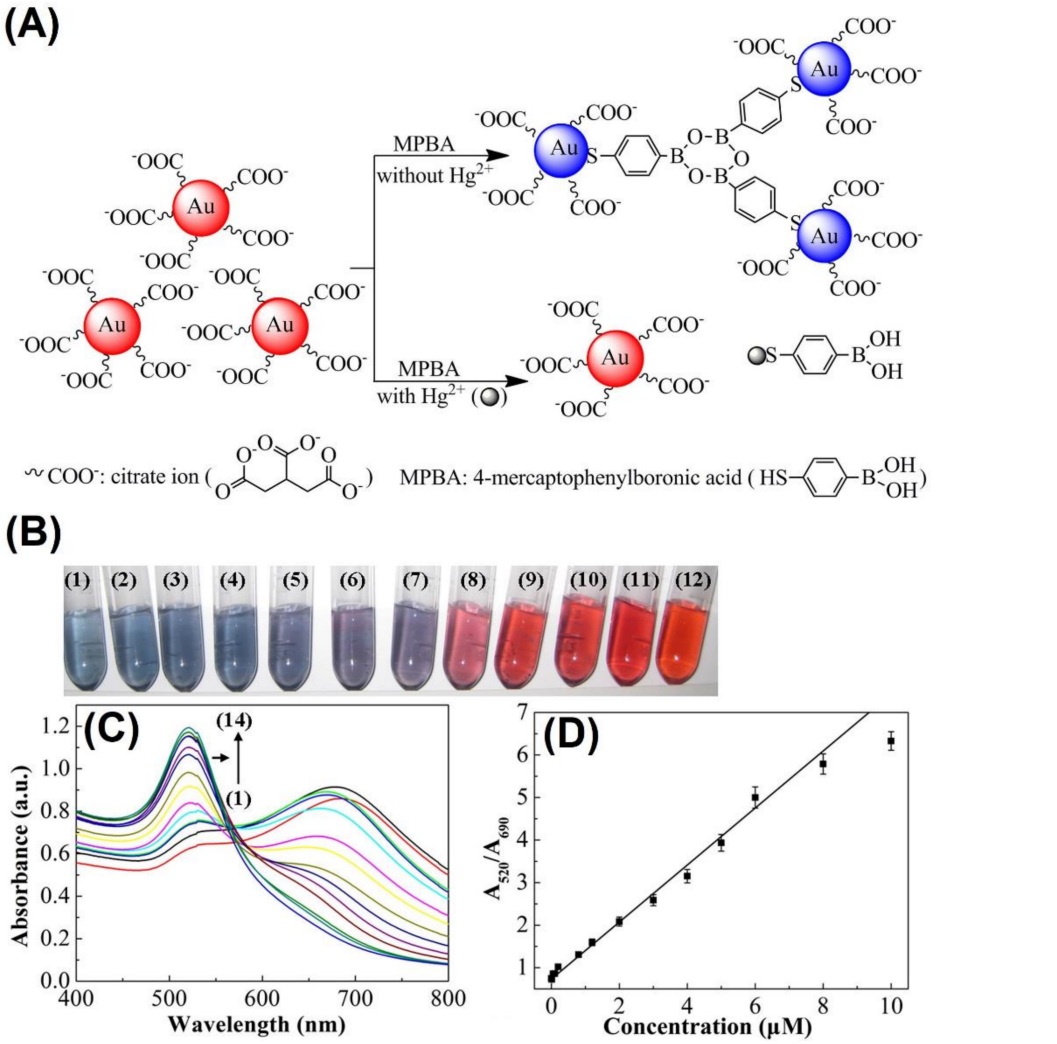

Figure 4. (**A**) Schematic presentation of the Au NPs colorimetric mechanism for Hg^{2+} detection; (**B**) photographic image; (**C**) UV–vis absorbance spectra and (**D**) linear plot of the A_{520}/A_{690} vs. Hg^{2+} concentration (c) of the MPBA (10 µM)-Au NPs solution (pH 4.0) containing various concentrations of Hg^{2+}: (1) 0, (2) 0.01, (3) 0.05, (4) 0.1, (5) 0.2, (6) 0.8, (7) 1.2, (8) 2, (9) 3, (10) 4, (11) 5, (12) 6, (13) 8, and (14) 10 µM. ((**A**–**D**) are reproduced with the permission from [52]).

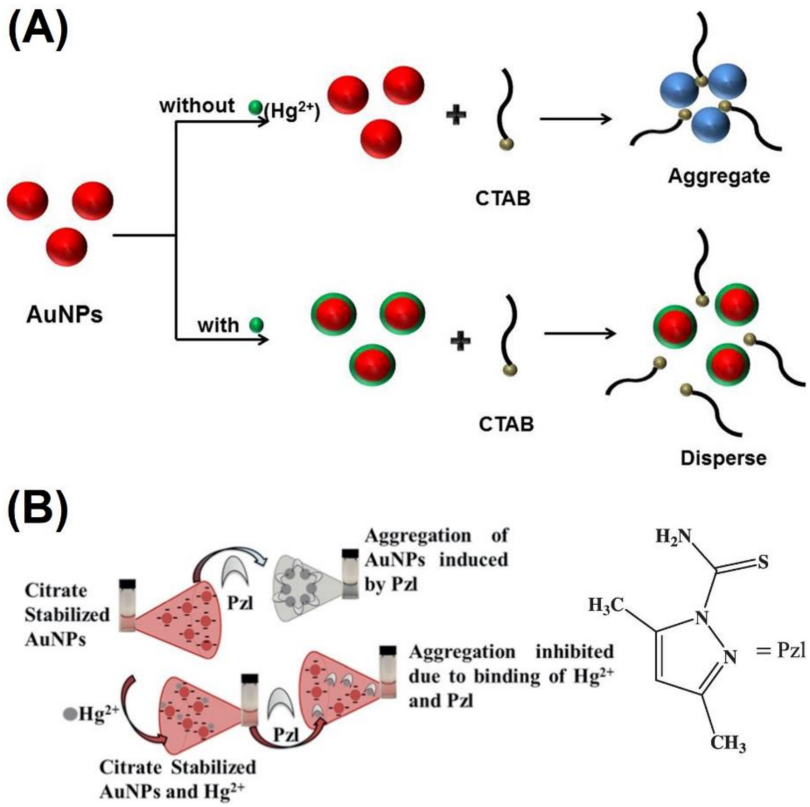

Figure 5. (**A**) The sensing mechanism of the colorimetric sensor based on anti-aggregation of Au NPs for Hg^{2+} detection (reproduced with the permission from [56]) and (**B**) schematic representation of the 3, 5-dimethyl-1-thiocarboxamidepyrazole (Pzl)-derived colorimetric detection mechanism for Hg^{2+} (reproduced with the permission from [57]).

Other than the Hg^{2+} detection, anti-aggregation-mediated discrimination of Ag^{+} was also demonstrated with CI-Au NPs, as described next. Mao et al. described CI-Au NPs' (particle size = 13 nm) anti-aggregation-tuned selective detection of Ag^{+} [58]. Herein, the thiamazole (2 μM) was used as an aggregation-inducing agent to produce an Au NPs color change from red to blue. The aggregation was then inhibited in the presence of Ag^{+}. Due to Ag^{+}-enhanced oxidization of sulfhydryl groups (-SH), anti-aggregation takes place to reverse the color from blue to red, as illustrated in Figure 6A. TEM study confirmed the involvement of the anti-aggregation strategy with the optimum pH value and response time fixed at 7.5 (buffer: Britton Robison (BR) buffer solution made up from H_3PO_4, H_3BO_3, and HAc (0.04 M)) and 15 min. The dynamic linear range of Ag^{+} was between 0.1 nM and 90 μM (at A_{520}/A_{660}), with an LOD of 0.042 nM. Note that there was no interfering effect in the presence of other ions, and real water (tap and river) samples displayed recoveries of >98%. This is a nice work (toward Ag^{+} quantification) in terms of its performance in the linear range, LODs, and real-time applicability.

Label-free Au NPs (particle size = 12 nm; synthesized via $NaBH_4$ reduction; SPR at 512 nm; conc. = 20 nM) composited with ascorbic acid (AA) were engaged in Ag^{+} detection without employing any aggregation agent [59]. The AA-tuned reduction of Ag^{+} resulted in Ag^{0} on Au NPs' surface and formed an Ag–Au alloy. The linearity of Ag^{+} was between 2 and 28 μM (SPR at 385 nm), with a calculated LOD of 0.85 μM. Even though this work was demonstrated in drinking water samples, it cannot be categorized as an anti-aggregation strategy-based sensor. Colorimetric detection of Ag^{+} based on anti-aggregation of CI-Au NPs (particle size = 20 nm; conc. = 1.2 nM) was proposed by Safavi and co-workers [60], wherein tris(hydroxymethyl) aminomethane (tris at 9 mM; pH 7.5) was used as the aggregation-inducing agent to deliver a color change from red to blue, with a new SPR peak occurring at 650 nm. The anti-aggregation-enabled colorimetric response is

observed with a color change from blue to red (within 20 min) due to the strong interaction between tris and Ag^+, as represented in Figure 6B. The Ag^+-mediated anti-aggregation was well established from TEM, SPR, and interference studies. The color change (from blue to red), SPR changes, linear range (1–9 μM; at A_{520}/A_{650}), and LOD (0.42 μM) calculations are shown in Figure 6C–E. This work was demonstrated by wastewater and river water investigations with a recovery >96%; therefore, it can be regarded as a nice innovation.

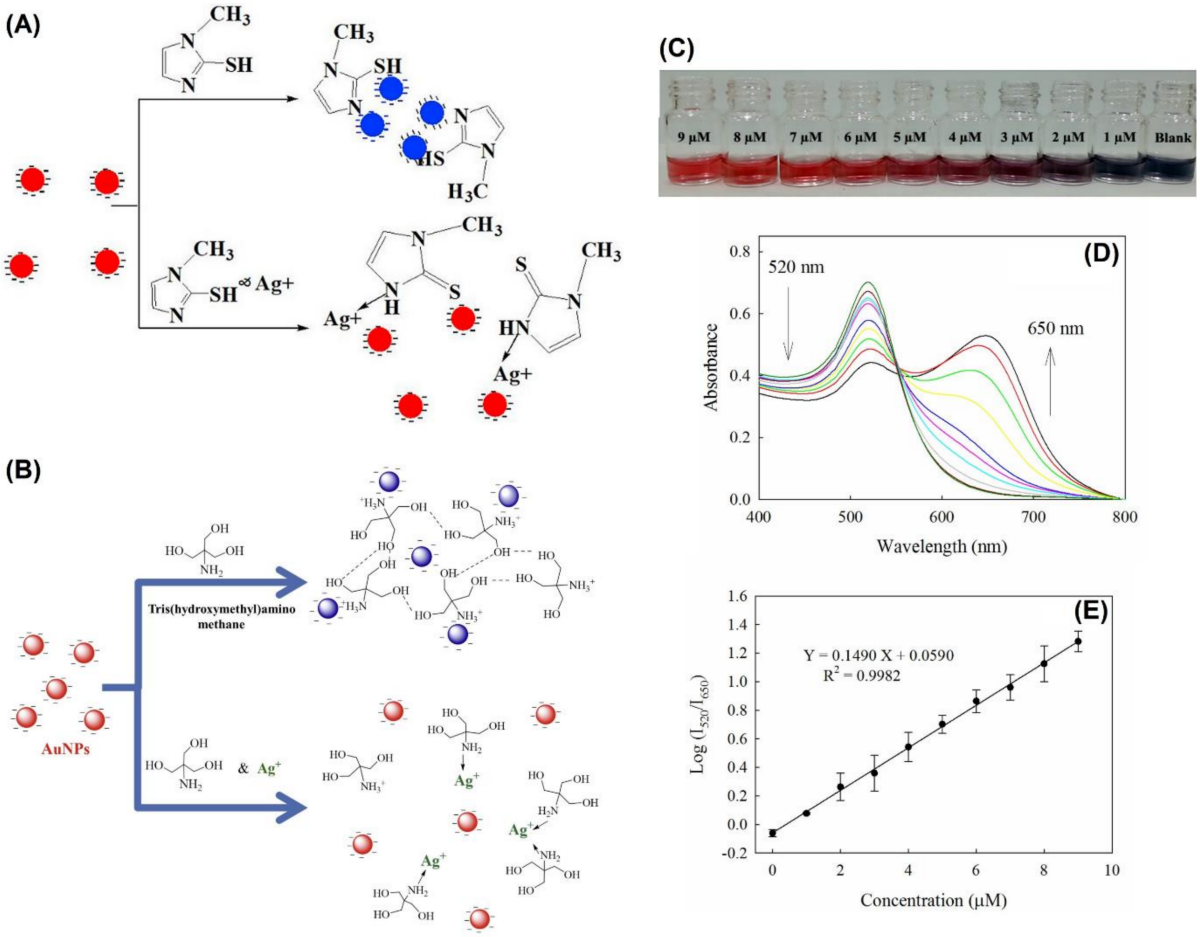

Figure 6. (**A**) Schematic representation of the analytical process for Ag^+ detection (reproduced with the permission from [58]); (**B**) schematic representation of the Au NPs-based colorimetric assay for silver; (**C**) color changes with increasing concentration of Ag^+ from 0 to 9 μM; (**D**) SPR absorption change of Au NPs in tris solution with Ag^+ concentration varied from 0 to 9 μM; (**E**) the linear response of the system to Ag^+ ion concentration. (The concentration of tris solution was 9 mM, and the pH was fixed at 7.5. Au NPs' concentration was 1.2 nM.) ((**B**–**E**) are reproduced with the permission from [60]).

Gao et al. described the anti-aggregation-facilitated detection of Cu^{2+} using CI-Au NPs (particle size = 18 nm; conc. = 3.89 nM) with glutathione (GSH; 5 μM) as the aggregation-inducing agent [61]. The free thiol (-SH) of GSH replaced the citrate from the Au NPs' surface to induce the aggregation in a short time and produced a color change from red to blue with a corresponding SPR shift from 520 nm to 650 nm. In the presence of Cu^{2+}, the GSH was oxidized to form GSSG, and the anti-aggregation took place to reverse the color from blue to red, with a shifting of the SPR peak from 650 nm to 520 nm. The best result was obtained at pH 3.4 (buffer: 4 mM BR) after 15 min incubation. It displayed a linear regression of between 20 and 500 nM (at A_{650}/A_{520}), with an LOD of 20 nM with Cu^{2+}, and was also demonstrated by tap water recovery (>96%; RSD $\leq$ 3%). Moreover, colorimetric reversibility of Cu^{2+} with S^{2-} was also discussed in this report.

Therefore, based on TEM, colorimetric/SPR responses, interference, kinetic, temperature, and reversibility investigations, this report can be attested as an exceptional work in Cu^{2+} detection. Thereafter, D-penicillamine (D-PC; 30 μM)-enabled aggregation of CI-Au NPs (particle size = 13 nm; conc. = 15 nM) was demonstrated in detecting Cu^{2+} via the anti-aggregation strategy [62]. The D-PC induced the aggregation via providing its free -SH unit to CI-Au NPs, which resulted in a color change from red to blue. After adding Cu^{2+}, D-PC coordinated with Cu^{2+} to form dimeric complexes (D-PC-Cu-D-PC via the S-Cu-S bond) and enabled anti-aggregation to reverse the color change from blue to red. The best result was found at pH 7 (buffer: 1 M NaCl-10 mM NaOH) in the presence of 25 mM NaCl and after 12 min incubation. The linear range of Cu^{2+} was between 0.05 and 1.85 μM (at A_{520}/A_{650}), with an LOD of 30 nM. TEM and SPR studies confirmed the anti-aggregation. The real water (tap water, cascade water, and mineral water) interrogations showed recoveries of between 85 and 108% (RSD = 1.43–6.93%). Thus, this work can be adopted in real time detection of Cu^{2+}; however, careful optimizations on the concentrations of D-PC, NaCl, and pH are required.

In contrast to the aforementioned metal ion sensors in this section, Deng and co-workers described the Schiff base and Lewis acid–base interaction-regulated anti-aggregation for colorimetric detection of Sc^{3+} [63], wherein the biomolecule pyridoxal phosphate (PLP; 5 μM; contains free -CHO group) reacted with cysteamine-functionalized Au NPs (Cyst-GNPs; particle size = 17.5 ± 3.4 nm (n = 100) positively charged with free $-NH_3^+$ at pH 6) to form a neutral Schiff base and induced aggregation to produce a color change from red to blue. The competition between the intense Lewis acid–base interactions of Sc^{3+} with PLP and Cyst-GNPs binding to PLP enables the anti-aggregation of Cyst-GNPs to display a reversed color change from blue to red, as shown in Figure 7. TEM, DLS, and SPR responses, and interference studies confirmed the anti-aggregation-based high selectivity of Sc^{3+}. The incubation time of all experiments was established as 1 min at pH 6 (buffer: HAc-NaAc). The linear regression of Sc^{3+} was between 0.1 and 3 μM (at A_{700}/A_{525}), with an estimated LOD of 20 nM. The tap water recoveries of Sc^{3+} in this method were between 96.87 and 101.8%, with corresponding RSD values of 0.6–3.6%. This is the only report in the anti-aggregation-mediated colorimetric detection of rare earth Sc^{3+}; therefore, it can be noted as an exceptional work. Table 1 delivers the linear ranges, LODs, pH (buffer), incubation time, and applications of anti-aggregation-enabled Au NPs-based colorimetric metal ion sensors reviewed in this section.

Table 1. Linear ranges, LODs, pH (buffer), incubation time, and applications of Au NPs-based probes reported in anti-aggregation-facilitated colorimetric detection of metal ions.

Probe	Aggregation-Inducing Agent; Optimum Conc.	Sensing Analyte	pH (Buffer); Incubation Time	Linear Range	Limit of Detection (LOD)	Applications	Ref.
CI-Au NPs	4,4′-Dipyridyl (DPy); 2.5 μM	Hg^{2+}	pH 7 (10 mM Tris–HCl); 30 min	0.04–1.1 μM	15 nM	Real water analysis	[47]
PDDA-Au NPs	Cysteine (Cys); 7 μg/mL in 0.1 M Na Cl	Hg^{2+}	pH 5 (HAc-NaAc); NA	0.05–10 μM	25 nM	Real water analysis	[48]
CI-Au NPs	Thymine; 0.2 mM	Hg^{2+}	pH 8 (1 mM Tris-HCl); 30 min	2–12 μM	2 nM	Real water analysis	[49]
CI-Au NPs	O-Phenylene-diamine (OPD); 3.1 μM	Hg^{2+}	pH 6.5 (NA); 20 min	0.01–2 μM	5 nM	Real water analysis	[50]
CI-Au NPs	L-Penicillamine (Pen); 3.5 μM	Hg^{2+}	pH 2.4 (5 mM citric acid–sodium citrate); 2 min	50–400 nM	25 nM	Real water analysis	[51]
CI-Au NPs	4-Mercapto-phenylboronic acid (MPBA); 10 μM	Hg^{2+}	pH 4(10 mM (5 mM citric acid–sodium citrate); 20 min	0.01–5 μM	8 nM	Real water analysis	[52]
CI-Au NPs	N-Acetyl-L-cysteine (NAC); 10 μM	Hg^{2+}	pH 7 (PBS); 30 min	0.02–1 μM	9.9 nM	Real water analysis	[53]
CI-Au NPs	2-Mercapto-benzothiazole (MBT); 2.2 μM	Hg^{2+}	pH 5.8 (PBS); 5 min	0.05–1 μM	6 nM	Real water and milk powder analysis	[54]
Tween 20 modified Au NRs	Dithiothreitol (DTT); 1.5 μM	Hg^{2+}	pH 7.4 (Tris–HCl); NA	1–100 pM	0.42 pM	Body fluid analysis	[55]

Table 1. *Cont.*

Probe	Aggregation-Inducing Agent; Optimum Conc.	Sensing Analyte	pH (Buffer); Incubation Time	Linear Range	Limit of Detection (LOD)	Applications	Ref.
CI-Au NPs	Hexadecyl trimethyl ammonium bromide (CTAB); 0.44 µM	Hg^{2+}	pH 7 (Tris–HCl); 30 min	0–0.68 µM	11.9 nM	Real water analysis	[56]
CI-Au NPs	3, 5-Dimethyl-1-thiocarboxamidepyrazole (Pzl); 1.5 µM	Hg^{2+}	Ph 5.6–8 (PBS); 3–4 min	0.01–1.5 µM	7.7 nM	Real water analysis	[57]
CI-Au NPs	Thiamazole; 2 µM	Ag^{+}	pH 7.5 (BR); 15 min	0.1 nM–90 µM	0.042 nM	Real water analysis	[58]
CI-Au NPs	Tris-(hydroxymethyl) aminomethane (Tris); 9 mM	Ag^{+}	pH 7.5 (Tris–HCl); 20 min	1–9 µM	0.41 µM	Real water analysis	[60]
CI-Au NPs	Glutathione (GSH); 5 µM	Cu^{2+}	pH 3.4 (4 mM BR); 15 min	20–500 nM	20 nM	Real water analysis	[61]
CI-Au NPs	D-Penicillamine (D-PC); at 25 mM NaCl	Cu^{2+}	pH 7 (1 M NaCl-10 mM NaOH); 12 min	0.05–1.85 µM	30 nM	Real water analysis	[62]
cysteamine-protected Au NPs	Pyridoxal phosphate (PLP); 5 µM	Sc^{3+}	pH 6 (HAc-NaAc); 1 min	0.1–3 µM	20 nM	Real water analysis	[63]

NA = Not available; min = minutes; mM = 10^{-3} M; µM = 10^{-6} M; nM = 10^{-9} M; pM = 10^{-12} M.

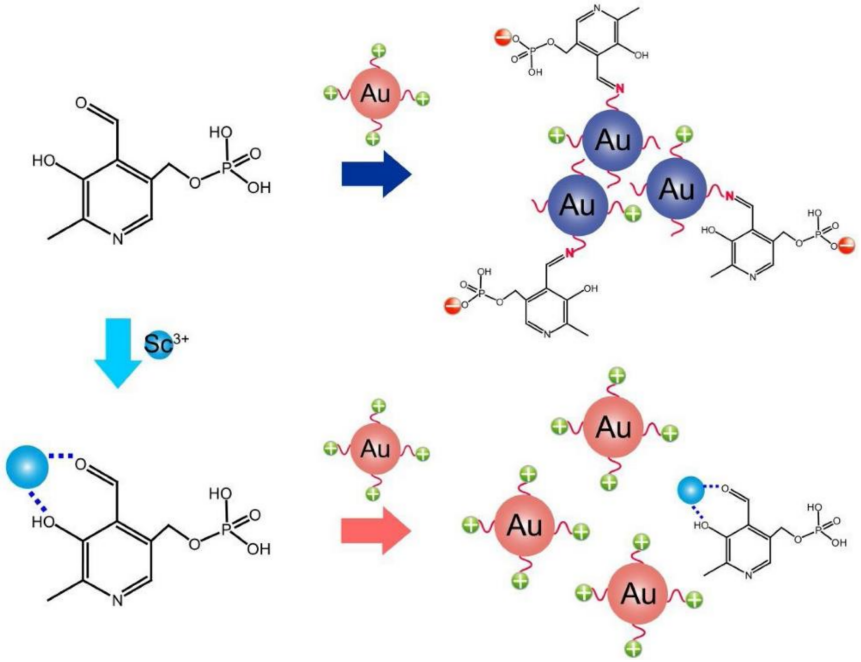

Figure 7. Schematic of PLP-triggered aggregation of Cyst-GNPs for colorimetric detection of Sc^{3+} (reproduced with the permission from [63]).

3. Au NPs-Based Colorimetric Quantification of Anions via Anti-Aggregation

Plaisen and co-workers described the detection of bromide anion (Br^{-}) via the anti-aggregation strategy [64] as follows: CI-Au NPs (particle size = 16.43 ± 0.81 nm; conc. = 5.52 nM) aggregation took place in the presence of Cr^{3+} ions (optimum conc. = 4.81 µM), which resulted in a color change from red to blue. However, when Br^{-} was pre-mixed (at pH 6.5 (buffer: 10 mM sodium phosphate (Na_3PO_4)) and 10 min reaction time), the color overturned from blue to red via anti-aggregation. TEM and DLS studies confirmed the involvement of the anti-aggregation strategy. In fact, Br^{-} tends to affect the citrate capping via self-deposition over the NPs' surface, which also hinders the binding of citrate to Cr^{3+}, thereby resulting in the color change. The linear regression of Br^{-} was found between to be 0.31 and 3.75 µM (at A_{519}/A_{673}), with an LOD of 40 nM and a limit of quantification (LOQ) of 0.13 µM. This work was applied in rice sample investigations; thus, it can be regarded as a nice innovation.

Due to the strong binding affinity of Hg^{2+} to the iodide anion (I^-), there are experiments and reports in using Hg^{2+} as an aggregation-inducing agent to conduct anti-aggregation-based colorimetric detection of I^-. The N-1-(2-mercaptoethyl) thymine-capped Au NPs (particle size = 23 nm; conc. = 1.4 nM), T-rich single-stranded DNA (DNA = deoxyribonucleic acid)-capped Au NPs, (T-rich ssDNA–Au NPs; particle size = 13; conc. = 3 nM), and 2-hydroxyethyldithiocarbamate-capped Au NPs (2heDTC-Au NPs; particle size = 12.92 ± 1.44 nm; conc. = 15 nM) were proposed in Hg^{2+}-enabled aggregation to engage in I^- detection via the anti-aggregation tactic [65–67]. The mercapto-functionalized thymine and T-rich ssDNA over Au NPs aggregated strongly in the presence of Hg^{2+} (300 nM and 2 μM, correspondingly) and induced color changes from red/wine-red to blue/violet-blue [65,66]. In fact, the aggregation is highly effective due to the strong attraction between thymine and Hg^{2+} via the T-Hg^{2+}-T complex. Upon pre-treating I^- with Hg^{2+}, the T-Hg^{2+}-T complexation was interrupted by the HgI_2 formation, thus reversing the colorimetric response from blue/violet-blue to red/wine-red via anti-aggregation. The best pH condition in both reports [65,66] was established as pH 7.4 (buffer: PBS and 20 mM Tris-HCl (contains 20 mM NaCl before addition), respectively) with a distinct incubation time of 5 min and 10 min, respectively. Figure 8A demonstrates the Hg^{2+}-induced aggregation and I^--enabled anti-aggregation of N-1-(2-mercaptoethyl) thymine-capped Au NPs. TEM, DLS, and SPR analysis attested to both aggregation (in the presence of Hg^{2+}) and anti-aggregation by I^-. Linear ranges of I^- by mercapto-functionalized thymine and T-rich ssDNA on Au NPs were determined as 10–600 nM (at A_{524}/A_{645}) and 40 nM–4 μM (at A_{520}/A_{650}), with LODs of 10 nM and 13 nM, respectively. Both reports show high selectivity and exceptional recoveries (>89%) in real water and human urine samples; thus, they can be regarded as good works.

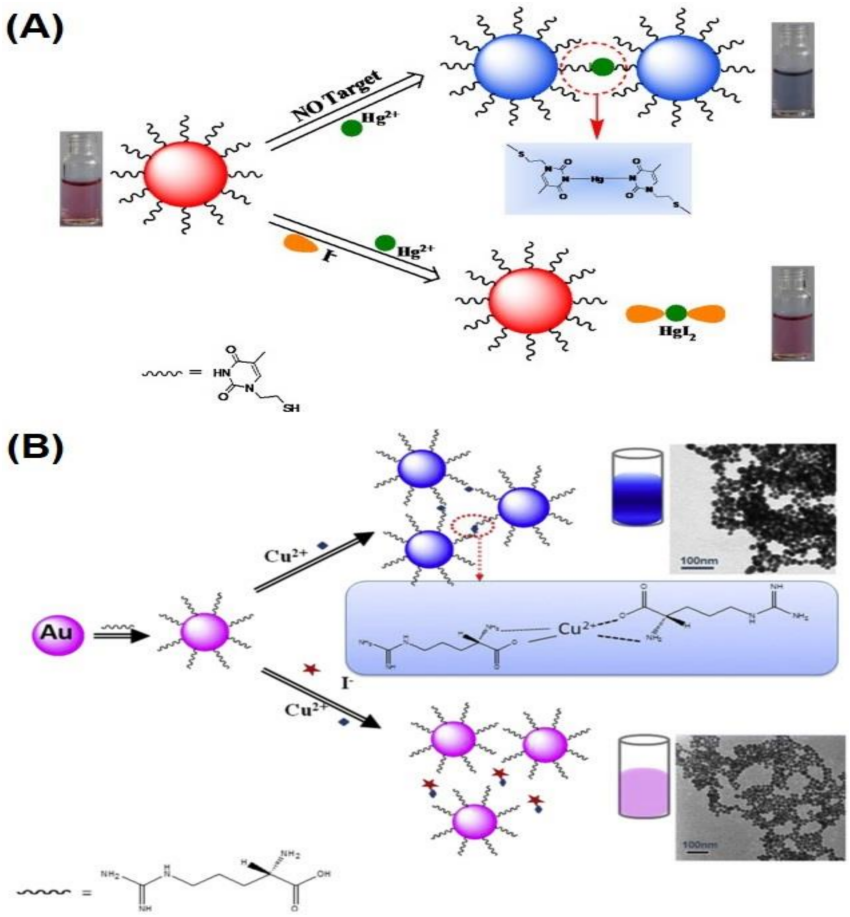

Figure 8. (**A**) Schematic illustration of the analytical process for detecting iodide based on the anti-aggregation of N-1-(2-mercaptoethyl) thymine-capped Au NPs (reproduced with the permission from [65]) and (**B**) schematic illustration of the sensing mechanism based on the arginine-capped Au NPs and Cu^{2+} (reproduced with the permission from [68]).

Subsequently, the 2heDTC-Au NPs also aggregated and induced a color change from red to blue in the presence of Hg^{2+}. The aggregation was interrupted in the presence of I^- with a reverse color change from blue to red via anti-aggregation [67]. The citrate on Au NPs were firstly modified via ligand exchange with 2-hydroxyethyldithiocarbamate (2heDTC), and then the interaction of Hg^{2+} with 2heDTC resulted in aggregated bare Au NPs. When I^- was added, the interaction of 2heDTC to Hg^{2+} was inhibited, and anti-aggregation occurred as supported by TEM, DLS, and SPR studies. The optimum pH and incubation time for this sensory study were fixed as pH 5 (buffer: 50 mM PBS) and 7 min. The linear regression of I^- was between 0.1 and 4 µM (at A_{520}/A_{650}), with an LOD of 20 nM. This work showed recoveries of >85% in edible salts; thus, it can be regarded as a unique colorimetric sensor for I^- quantification.

In this track, the arginine-capped Au NPs (Arg-Au NPs; particle size = 13 nm) were utilized for detecting I^- via anti-aggregation by engaging Cu^{2+} (70 µM) as the aggregation-inducing agent [68]. In the presence of Cu^{2+}, the Arg-Au NPs began to aggregate with a colorimetric response from red to blue via Arg-Cu^{2+}-Arg complexation. The dimeric Arg-Cu^{2+} complex was disturbed by adding I^- to induce the anti-aggregation and produce a colorimetric response from blue to red. The actual reaction between Cu^{2+} and I^- is represented by Equation (1) and schematically illustrated in Figure 8B:

$$2Cu^{2+} + 4I^- = 2CuI + I_2 \quad (1)$$

The best pH condition and incubation time were established as pH 7.4 (buffer: PBS) and 5 min. TEM, DLS, and SPR analysis also confirmed involvement of the anti-aggregation. The linear range of I^- was between 0.01 and 4 µM (at A_{524}/A_{654}), with an LOD of 10 nM. Drinking water and table salt investigations showed recoveries of between 96 and 108% and 94 and 103%, respectively, with RSD values of <3.9%. Though this work was effective in I^- quantitation, further optimizations on the Cu^{2+} concentrations are still required in future work. By means of anti-aggregation, CI-Au NPs were engaged for the colorimetric detection of I_2 using thiosulfate ($S_2O_3^{2-}$; 5.94 mM) as an aggregation-inducing agent [69]. Initially, Au NPs react with $S_2O_3^{2-}$ to form a strong Au-S bond and to induce aggregation of NPs (with a color change from red to blue). Then a redox reaction takes place toward the formation of $Au(S_2O_3)_2^{3-}$, as described below in Equation (2):

$$4Au + O_2 + 2H_2O + 8\,S_2O_3^{2-} \rightarrow 4[Au(S_2O_3)_2]^{3-} + 4\,OH^- \quad (2)$$

Upon pre-incubating I_2 with Au NPs, the free thiosulfate is produced due to another redox reaction between I_2 and $S_2O_3^{2-}$, as described in Equation (3). Thereafter, anti-aggregation takes place to induce the color from blue to red.

$$I_2 + {S_2O_3^{2-}}_{(aq)} \rightarrow 2{I^-}_{(aq)} + {S_4O_6^{2-}}_{(aq)} \quad (3)$$

TEM and SPR interrogations well attested the anti-aggregation strategy. The best result was achieved at pH 7 after 16 min incubation. The linear range of I_2 was between 3 and 80 nM (at A_{519}/A_{640}), with an LOD of 1.36 nM. Moreover, plasma and tap water investigations showed >97% recovery. However, this work still needs more experimental data on the particle size variations, DLS, and interference studies.

Deng et al. described the anti-aggregation-enabled detection of thiocyanate anion (SCN^-) by engaging CI-Au NPs (particle size = 13 nm; conc. = 3.2 nM) and 8 mM of sulfuric acid (H_2SO_4) as the aggregation-inducing agent [70]. In the presence of H_2SO_4 (8 mM), the Au NPs aggregated with a simultaneous color variation from red to blue. When SCN^- was added, anti-aggregation (via forming Au-S bonds) was induced to produce a blue-to-red color change, which was validated by SPR and TEM studies. The SCN^- displayed a linear regression of between 0.25 and 2 µM (at A_{700}/A_{520}), with an LOD of 0.14 µM. Intensity of the color was visible to naked eyes at 1 µM concentration. The tap water recoveries ranged between 94.8 and 101.3%, with RSDs of 1.6–3.2%. It should be noted that this work

validated the selectivity of SCN^- over a wide range of cations and anions. However, further study is mandatory to improve the LOD toward nM or PM. Moreover, its applicability requires justification due to the use of an acidic aggregation-inducing agent. Song and co-workers described the anti-aggregation-enabled detection of SCN^- by employing CI-Au NPs (particle size = 13 nm) and cetyltrimethyl ammonium bromide (CTAB; 0.5 μM) as the aggregation-inducing agent [71]. Due to the strong electrostatic interaction between CTAB and stabilizing agent citrate, the aggregation induced a color change from red to blue. When SCN^- was added, it strongly coordinated with the Au surface with a high stability constant; thus, Au NPs were re-dispersed via anti-aggregation and displayed a color change from blue to red. The SPR, color change, and nanoparticles size variations during subsequent interaction of CTAB and SCN^- are displayed in Figure 9A,B.

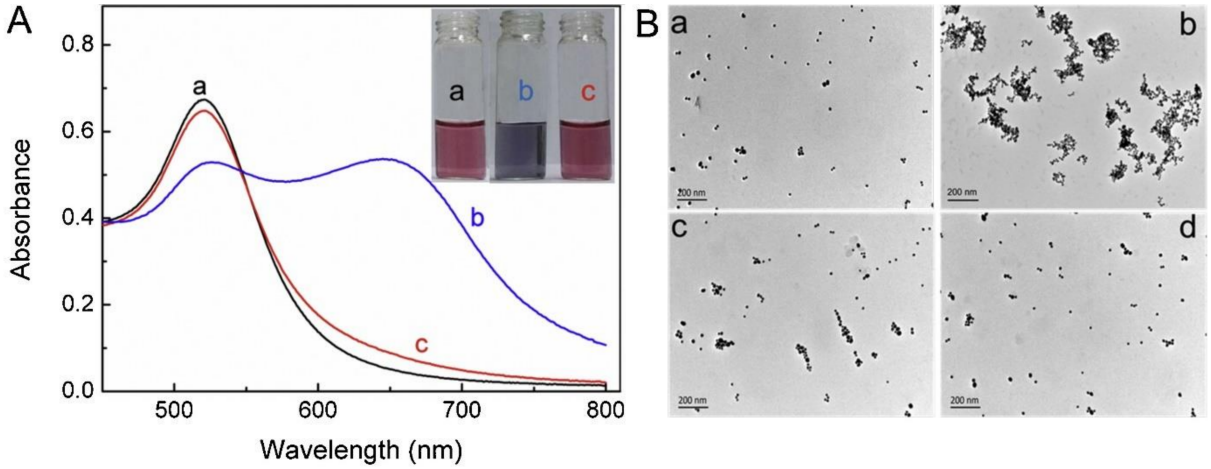

Figure 9. (**A**) UV−vis spectra and colors of Au NPs in the absence (a) and presence of 0.5 μM CTAB (b), after the addition of 0.5 μM CTAB and 1.5 μM SCN^- (c). (**B**) TEM images of Au NPs, naked Au NPs (**a**), and Au NPs with 0.5 μM CTAB: in the presence of 0 (**b**), 1.5 μM (**c**), and 2.0 μM SCN^- (**d**); scale bars for (**a**–**d**) = 200 nm ((**A**,**B**) are reproduced with the permission from [71]).

The probe had a high selectivity over a wide range of analytes and showed the best sensory performance to SCN^- at pH 7 (buffer: 10 mM PBS) after 15 min incubation. The linearity of SCN^- ranged between 0.1 and 1.5 μM (at A_{650}/A_{520}), with an LOD of 6.5 nM. Real studies on solid and liquid milk samples demonstrated a recovery of >90% with an RSD of ≤5.5%. Based on the selectivity, sensitivity, and real samples investigations, this work can be regarded as nice invention for SCN^- monitoring in real-time. By employing the 2-amino pyridine (2-AP; 50 μM) as the aggregation-inducing agent, CI-Au NPs (particle size = 10–44 nm; conc. = 8.3 nM) were engaged in detecting SCN^- [72]. In this work, the +vely charged 2-AP interacted with -vely charged CI-Au NPs to form the static electricity and to induce the aggregation with a color change from red to blue. Due to the strong binding affinity of SCN^- to Au NPs (via Au-S bond), the 2-AP-induced aggregation was disturbed, which resulted in the dispersion of Au NPs via anti-aggregation as evident from a color change from blue to red and SPR, DLS, and TEM studies. The optimum anti-aggregation induced by SCN^- occurred at pH 7 (buffer: 40 mM Tris-HCl) and displayed a linearity of between 0.4 and 1.2 μM (at A_{675}/A_{520}), with an LOD of 0.37 μM. Tap water investigations demonstrated recoveries of between 98.52 and 105.48%, with an RSD of <4.6%. Though the sensitivity of this work is high, further optimization is required to tune the LOD toward the nM level.

Lu et al. described the use of dithiothreitol (DTT; 4 μM) as an aggregation-inducing agent with CI-Au NPs (particle size = 13 nm; 11 nM) to quantify the hypochlorite (OCl^-) anion via the anti-aggregation strategy [73], wherein the DTT with a free thiol unit at both ends enabled aggregation of Au NPs and displayed a color change from red to blue. Upon adding OCl^-, a redox reaction takes place to oxidize the DTT (6-electron transfer process) to its sulfonate derivatives, which results in anti-aggregation of Au NPs with a color

change from blue to red, as depicted in Figure 10A. The optimum condition for colorimetric detection of OCl^- was at pH 7.17 (buffer: 45 mM PBS), with incubation time of 2 min. Photographs and SPR, TEM, and XPS (XPS = X-ray photoelectron spectroscopy) studies attested to the anti-aggregation being induced by OCl^-. With the OCl^- concentrations between 0 and 7 μM, the SPR peak changes at A_{665}/A_{520}, with an LOD of 2 μM, could be visualized with naked eyes. Figure 10B,C display the SPR and colorimetric changes as a function of the OCl^- concentration (0–8 μM). It should be noted that none of the interfering species could affect the OCl^- selectivity. Moreover, real water (tap water/lake water) investigations displayed a recovery >80%. However, this work lacks UV-based LOD calculations and DLS interrogations.

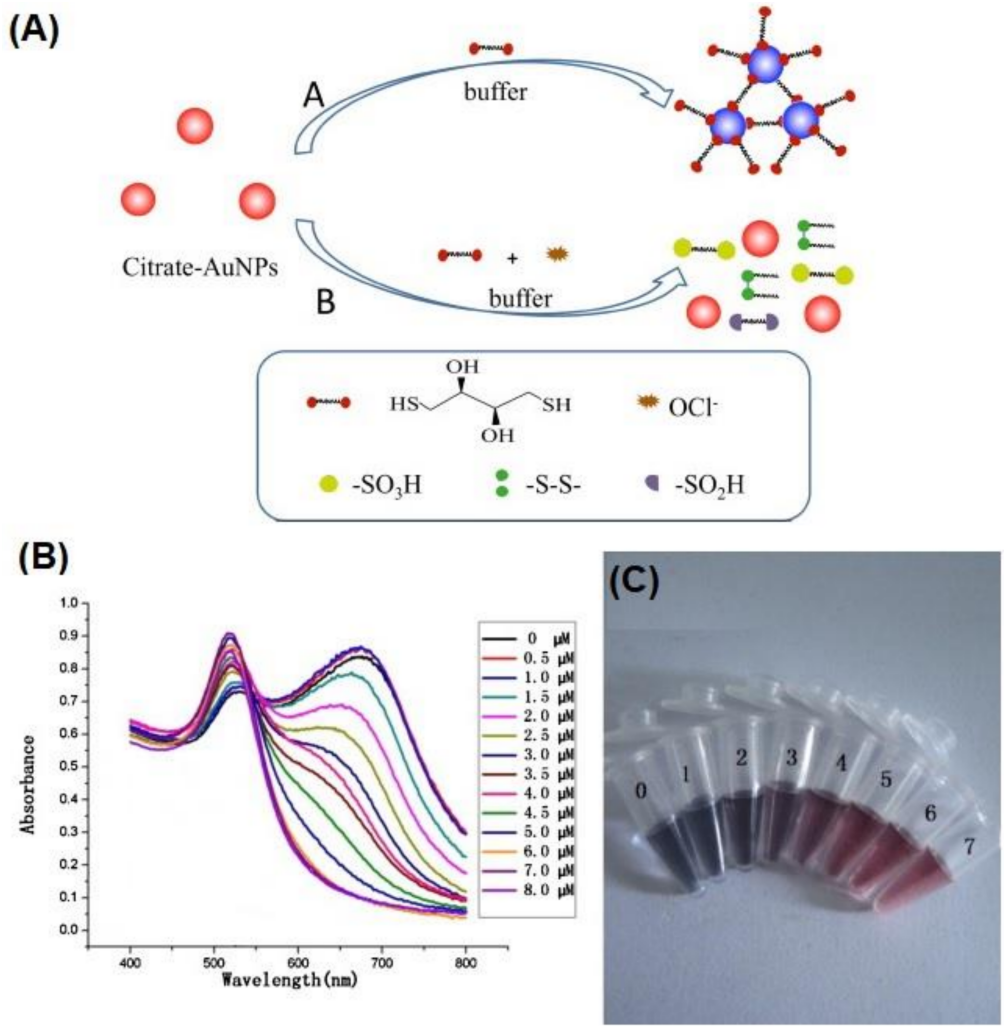

Figure 10. (**A**) Schematic representation of the hypochlorite sensor with unmodified gold nanoparticles; (**B**) optical absorption spectra in the presence of different concentrations of hypochlorite. Conditions: PBS (10 mM, pH 7.17), DTT (4.0 μM), and (**C**) photographs showing the colorimetric responses (the hypochlorite concentrations, in μM, are listed on the centrifuge tubes) ((**A**–**C**) are reproduced with the permission from [73]).

Liu and co-workers synthesized the mercapto–acetic acid–capped Au NPs (MA-Au NPs; particle size = 13 nm; conc. = 3 nM) and were employed in the detection of phosphate (PO_4^{3-}; Pi) anions via the anti-aggregation tactic [74] in which the Eu^{3+} (20 μM) was used as the aggregation-inducing agent. Adding the Eu^{3+} to MA-Au NPs induced aggregation and a color change (from red to blue) because of the effective coordination with free carboxyl (-COOH) units of mercapto–acetic acid. Pre-mixing of Pi anion into the above mixed system inhibits formation of -COOH-Eu^{3+} complex via strong Pi-Eu^{3+} binding, as seen in Figure 11.

TEM and SPR studies confirmed the anti-aggregation, and the best pH and incubation time were determined as pH 7.4 (buffer: 25 mM Tris-HCl) and 5 min. The linear range of Pi was between 0.5 and 30 μM (at A_{520}/A_{670}), with an LOD of 76 nM. Real samples studies demonstrated selectivity over other interferences but lacked spiked recovery investigations. However, this is the only report available which is based on anti-aggregation of Au NPs.

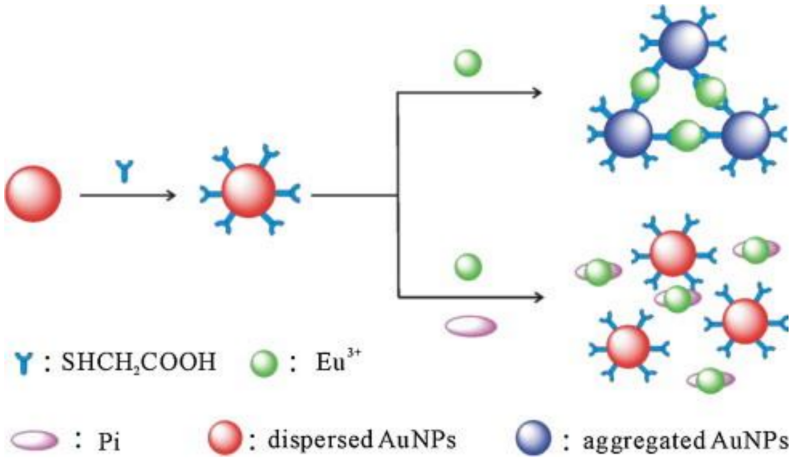

Figure 11. Schematic representation of the colorimetric assay of Pi based on anti-aggregation of MA-Au NPs (reproduced with the permission from [74]).

The CI-Au NPs (particle size = 13 nm) were also engaged in anti-aggregation-enabled detection of the nitrite anion (NO_2^-) using 4-Amino-thiophenol (4-ATP; 25 μM) as the aggregation-inducing agent. Herein, the 4-ATP induced aggregation (with a color change from red to blue) via a coating on Au NPs' surface; however, the diazonium reaction with NO_2^- disturbed the aggregation and led to a blue-to-red color change. To attain the best result, the pH, H_2SO_4 concentration, and incubation time were fixed as pH 9.5 (buffer: Na_2CO_3–$NaHCO_3$), 100 mM H_2SO_4 (catalytic amount of 10 μL from 1M stock) and 15 min, respectively. SPR, TEM, and interference studies validated the proposed tactic for NO_2^- quantitation. The linear range of NO_2^- was between 1 and 25 μM (at A_{685}/A_{520}), with an LOD of 1 μM. Spiked ground water and tap water investigations on the NO_2^- quantification showed recoveries of >98%, with an RSD of ≤8%, thereby confirming the practicality of this method. Based on the available data, this report can be regarded as an exceptional work for the NO_2^- assay. Table 2 provides information of the linear ranges, LODs, pH (buffer), incubation time, and applications of anti-aggregation-enabled Au NPs-based colorimetric anion sensors reviewed in this section.

Table 2. Linear ranges, LODs, pH (buffer), incubation time, and applications of Au NPs-based probes reported in anti-aggregation-enabled colorimetric detection of anions.

Probe	Aggregation-Inducing Agent; Optimum Conc.	Sensing Analyte	pH (Buffer); Incubation Time	Linear Range	Limit of Detection (LOD)	Applications	Ref.
CI-Au NPs	Cr^{3+}; 4.81 μM	Br^-	pH 6.5 (10 mM Na_3PO_4); 10 min	0.31–3.75 μM	40 nM	Rice samples analysis	[64]
N-1-(2-mercaptoethyl) thymine-capped Au NPs	Hg^{2+}; 300 nM	I^-	pH 7.4 (PBS); 5 min	10–600 nM	10 nM	Real water analysis	[65]
T-rich single-stranded DNA–capped Au NPs	Hg^{2+}; 2 μM	I^-	pH 7.4 (10 mM Tris-HCl); 10 min	40 nM–4 μM	13 nM	Real water analysis	[66]
2-hydroxyethyldithiocarbamate-capped Au NPs	Hg^{2+}; 2 μM	I^-	pH 5 (50 mM PBS); 7 min	0.1–4 μM	20 nM	Edible salt analysis	[67]
Arginine-capped Au NPs	Cu^{2+}; 70 μM	I^-	pH 7.4 (PBS); 5 min	0.01–4 μM	10 nM	Real water analysis	[68]
CI-Au NPs	$S_2O_3^{2-}$; 5.94 mM	I_2 (Iodine)	pH 7 (NA); 16 min	3–80 nM	1.36 nM	Real water and plasma analysis	[69]
CI-Au NPs	H_2SO_4; 8 mM	SCN^-	NA; 5 min	0.25–2 μM	0.14 μM	Real water analysis	[70]

Table 2. *Cont.*

Probe	Aggregation-Inducing Agent; Optimum Conc.	Sensing Analyte	pH (Buffer); Incubation Time	Linear Range	Limit of Detection (LOD)	Applications	Ref.
CI-Au NPs	Cetyltrimethyl ammonium bromide (CTAB); 0.5 μM	SCN^-	pH 7 (10 mM PBS); 15 min	0.1–1.5 μM	6.5 nM	Milk samples analysis	[71]
CI-Au NPs	2-Aminopyridine; 50 μM	SCN^-	pH 7 (40 mM Tris-HCl); NA	0.4–1.2 μM	0.37 μM	Real water analysis	[72]
CI-Au NPs	Dithiothreitol (DTT); 4 μM	OCl^-	pH 7.17 (45 mM PBS); 2 min	0–7 μM	2 μM (by naked eyes)	Real water analysis	[73]
Mercapto–acetic acid–capped Au NPs	Eu^{3+}; 20 μM	PO_4^{3-} (Pi)	pH 7.4 (25 mM Tris-HCl); 5 min	0.5–30 μM	76 nM	NA	[74]
CI-Au NPs	4-Amino-thiophenol (4-ATP); 25 μM	NO_2^-	pH 9.5 (Na_2CO_3–$NaHCO_3$); 15 min	1–25 μM	1 μM	Real water analysis	[75]

NA = Not available; min = minutes; mM = 10^{-3} M; μM = 10^{-6} M; nM = 10^{-9} M.

4. Au NPs-Based Colorimetric Quantification of Bio-Analytes via Anti-Aggregation

Au NPs-based colorimetric assays of biothiols, such as glutothione (GSH), cysteine (Cys), and homo-cysteine (HCys), via anti-aggregation were described by employing 4-(2-mercaptoethylamino)-1,8-naphthalimide–capped Au NPs (particle size = 10–20 nm; conc. = 5 nM) in the presence of Hg^{2+} (4.5 μM; aggregation-inducing agent) [76]. At an optimized concentration of capping agent "4-(2-mercaptoethylamino)-1,8-naphthalimide (9 μM)", Au NPs aggregated in the presence of Hg^{2+} through the T-Hg^{2+}-T complex (T exist in the naphthalimide unit) with a color change from red to blue. Above aggregation was hindered by pre-mixing GSH, Cys, and HCys with Hg^{2+} at an optimum pH 7.4 (buffer: 50 mM PBS) and 20 min incubation to induce anti-aggregation of Au NPs (due to strong biothiols-Hg^{2+} complex via Hg-S bond) and a color change from blue to red. TEM, SPR, and interference interrogations clarified the occurrence of anti-aggregation and high selectivity. The linear ranges of GSH, Cys, and HCys were between 0.025 and 2.28 μM (at A_{528}/A_{615}), 0.035 and 1.53 μM (at A_{528}/A_{615}), and 0.040 and 2.20 μM (at A_{528}/A_{615}), with LODs of 17 nM, 9 nM, and 18 nM, respectively. Spiked human urine studies established recoveries of >93% with an RSD of <5.5%; thus, it can be regarded as an excellent innovation.

Li et al. adopted the "S-adenosyl-L-methionine" (SAM; 0.8 μM) as an aggregation-inducing agent with CI-Au NPs (particle size = 10–20 nm; conc. = 3.5 nM) toward the quantification of biothiols (GSH, Cys and HCys) [77]. Firstly, adding SAM neutralized the potential of dispersed Au NPs and resulted in the aggregation with a color change from red to blue. Pre-treating biothiols with SAM disturbed the aggregation by displacing SAM from the NPs' surface via strong Au-S binding, thereby changing the color from blue to red. The optimum pH and incubation time were fixed as pH 7 (buffer: 10 mM borate buffered saline (BBS) made up from sodium borate and NaCl) and 5 min. TEM and SPR investigations attested to the anti-aggregation induced by biothiols. The linear regressions of GSH, Cys, and HCys were between 0.2 and 0.9 μM (at A_{520}/A_{650}), 0.4 and 1.2 μM (at A_{520}/A_{650}), and 0.6 and 3.0 μM (at A_{520}/A_{650}), with LODs of 35.8 nM, 21.7 nM, and 62.4 nM, correspondingly. This tactic shows high selectivity over a wide range of interferences, as seen in Figure 12, with recoveries in biological fluids of 96.5% to 104.4%; hence, it can be employed for real-time biothiols assay.

Zhong et al., 2010 and Wu et al., 2017 research groups demonstrated the anti-aggregation-enabled colorimetric assay of GSH using CI-Au NPs (particle size = 13 nm; conc. = 5/2.5 nM) with sodium piperazinebisdithiocarbamate (ppzdtc; 1.5 μM), cysteine (Cys; 4 μM), and 2-Mercapto-1-methylimidazole (MMI; 2 μM) as aggregation-inducing agents [78–80]. Initially, the aggregation-inducing agents functionalized on the surface of NPs reduced the electrostatic repulsion between NPs, which resulted in aggregation with a color change from red to blue. Pre-mixing of ppzdtc, Cys, and MMI with GSH led to anti-aggregation of Au NPs via a strong Au-S bond and kept the nanoparticles well-dispersed. When ppzdtc was used [78], the best pH value and incubation time were established as pH 7.4 (buffer: 10 mM HEPES

(4-(2-hydroxyethyl)-1-piperazineethanesulfonic acid)) and 30 min. In contrast, in the presence of Cys and MMI [79,80], the pH and incubation time for GSH assay were determined as pH 5.8 (buffer: PBS) and 5 min. TEM, DLS, and SPR analysis confirmed the anti-aggregation strategy in these reports. Figure 13A–D illustrate the proposed mechanism and changes in TEM in the presence of MMI and GSH [80]. The linear ranges of GSH were between 8 and 250 nM (at A_{520}/A_{640}), 0.1 and 1 μM (at A_{650}/A_{520}), and 0.1 and 1 μM (at A_{520}/A_{640}), with estimated LODs of 8 nM, 20.3 nM, and 12 nM, respectively. These three reports demonstrated the high selectivity of GSH over a wide range of interferences. In particular, the assay of GSH displayed high responses in the presence of Cys and H-Cys. From human serum and human urine investigations, recoveries of >90% were witnessed in Wu's reports [79,80]. Based on the obtained results, these Au NPs probes/tactics can be applied for GSH assay in real samples.

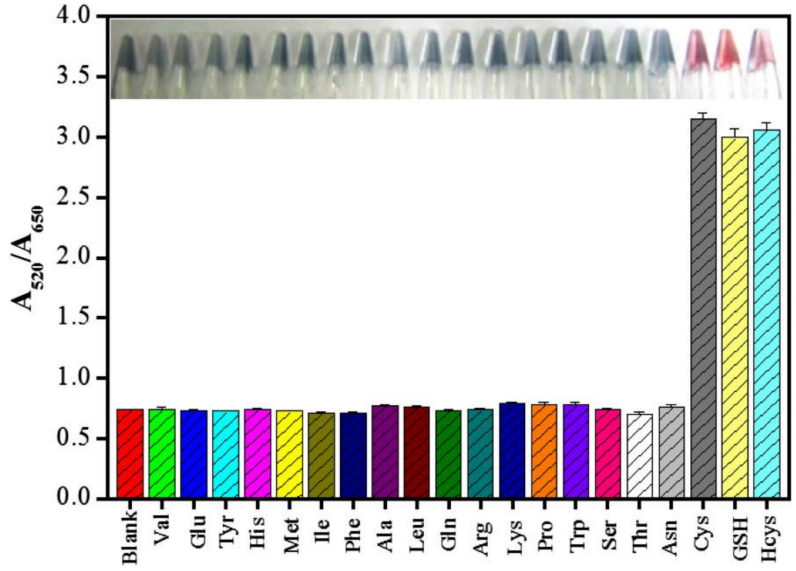

Figure 12. Absorbance ratio A520/A650 of solutions containing 3.5 nM of Au NPs, 0.8 mM of SAM, and 2 mM of different compounds and the target biothiols. The inset shows the corresponding photographic images of Au NPs (reproduced with the permission from [77]).

In the anti-aggregation-enabled colorimetric assay of D-aminoacids (DAAs; D-alanine (D-Ala)), the CI-Au NPs (particle size = 13 nm; conc. = 10 nM) and 4-mercaptobenzoic acid (4-MBA; 5.2 μM) with $CuCl_2$ (400 μM) were adopted as the probe and aggregation-inducing agent [81]. Both 4-MBA and Cu^{2+} induced aggregation of Au NPs with a color change from red to royal purple. In the presence of D-amino acid oxidase (DAAO), the DAAs were oxidized to produce hydrogen peroxide (H_2O_2), which took part in the oxidization of 4-MBA and formed the disulfide (-S-S-) bond. This process resulted in the anti-aggregation of Au NPs and a color change from royal purple to red. The best result was obtained at pH 7 (buffer: HAc-NaAc) after 15 min incubation. Being one of the D-aminoacids sources, the D-Ala was engaged in this study to demonstrate its selectivity in the presence of other interferences, such as vitamin C, glucose, Ca^{2+}, Mg^{2+}, Na^{+}, glycine (Gly), L-glutamic acid (L-Glu), L-alanine (L-Ala), and L-arginine (L-Arg). Colorimetric photographs and TEM and SPR studies confirmed the anti-aggregation by D-Ala. The linear range was between 0.15 and 30 μM (at A_{700}/A_{520}), with an LOD of 75 nM. This work was also demonstrated in real biological samples recovery (>98%). However, it still requires extra work to simplify the complicated procedure and to try out many distinct D-aminoacids.

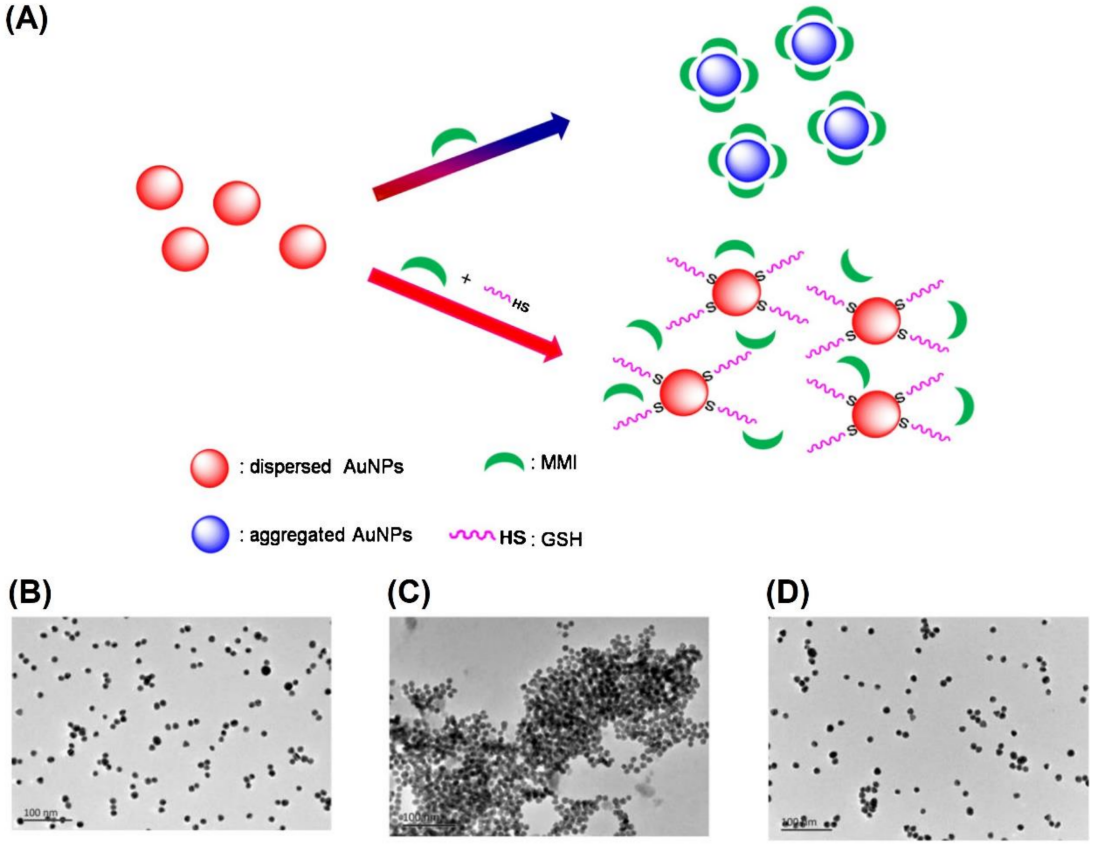

Figure 13. (**A**) Schematic representation of GSH-induced anti-aggregation of Au NPs with the use of MMI (MMI = 2-Mercapto-1-methylimidazole) as the aggregation agent and (**B**) TEM images of Au NPs only (**C**) in the presence of 2.0 μM MMI and (**D**) in the presence of 2.0 μM MMI and 1.0 μM GSH ((**A**–**D**) are reproduced with the permission from [80]).

Huang et al. discussed the anti-aggregation-facilitated colorimetric discrimination of methionine (Met) using CI-Au NPs (particle size = 13 nm; conc. = 15 nM) and melamine (Mel; 1.3 μM) as the aggregation-inducing agent [82]. Due to the strong Au-N binding, Mel induced aggregation of the NPs with a color change from red to blue. When Met was added, the above system was disrupted by means of strong Au-N and Au-S binding between Met to Au NPs (contrary to the Au-N bond in Mel-Au NPs), thereby enabling anti-aggregation to produce a colorimetric response from blue to red. The best colorimetric response was attained at pH 7.4 (buffer: PBS) after 5 min incubation. TEM, DLS, and SPR results attested to the anti-aggregation-enhanced colorimetric response. Note that none of the competing species showed interference. The NaCl at 20 mM in particular showed negligible effect on sensing. As explored in Figure 14A,B, the relative intensity of the two resonances in the SPR spectra of Mel-Au NPs system decreased linearly from 0 to 1 μM (at A_{650}/A_{520}), with an LOD of 24.5 nM. Human serum and human urine samples interrogations revealed recoveries on Met detection of between 5.0 and 105% and 95.0 and 104%, with an RSD of <5%. This is a unique work toward the colorimetric quantification of methionine and can be used for real-time quantification.

Keshvari and co-workers proposed the anti-aggregation-enabled colorimetric detection of fructose using CI-Au NPs (particle size = 13 nm) and 4-mercapto-phenyl boronic acid (MPBA; 1.34 μM) as the aggregation-inducing agent [83]. Due to the strong binding between the mercapto (-SH) unit and the Au atom, the aggregation occurred with a color change from ruby red to blue. When fructose was added, a borate ester was formed via a boronic acid-diol binding because of the reaction between boronic acid and cis-2,3-ribose diol (present in fructose), thereby inducing anti-aggregation of the NPs with a corresponding color change from blue to wine-red. The above reaction was dependent upon the pH

values, and the optimum value for the reaction to proceed was found to be pH 7. For collecting all colorimetric data, 10 min incubation was chosen. TEM and SPR analysis well proved the existence of anti-aggregation, and competing studies with many sugar carbohydrates (fructose, galactose, mannose, lactose, saccharose, and glucose, respectively) also confirmed its high selectivity. The linearity of fructose was between 32 and 960 μM (at A_{519}/A_{640}), with an LOD of 10 μM. The spiked human plasma investigation revealed recoveries of nearly 100%. However, this work requires more experimental data, including other interferences (such as uric acid, ascorbic acid, aminoacids, etc.), DLS, exact pH buffer used, NaCl effect, and real samples investigations. To this track, an anti-aggregation-enabled glucose sensor through localized surface plasmon resonance (LSPR) response on fiber optics was reported using amine@POSS-aminophenylboronic acid (APBA) immobilized on Au NPs' surface with the support of polyoligomeric silsesquioxane (POSS) [84], wherein a borate–glucose complex was responsible for the distinct LSPR responses. Though this work detects the glucose with an LOD of 25 μM, it lack colorimetric responses for in depth discussion.

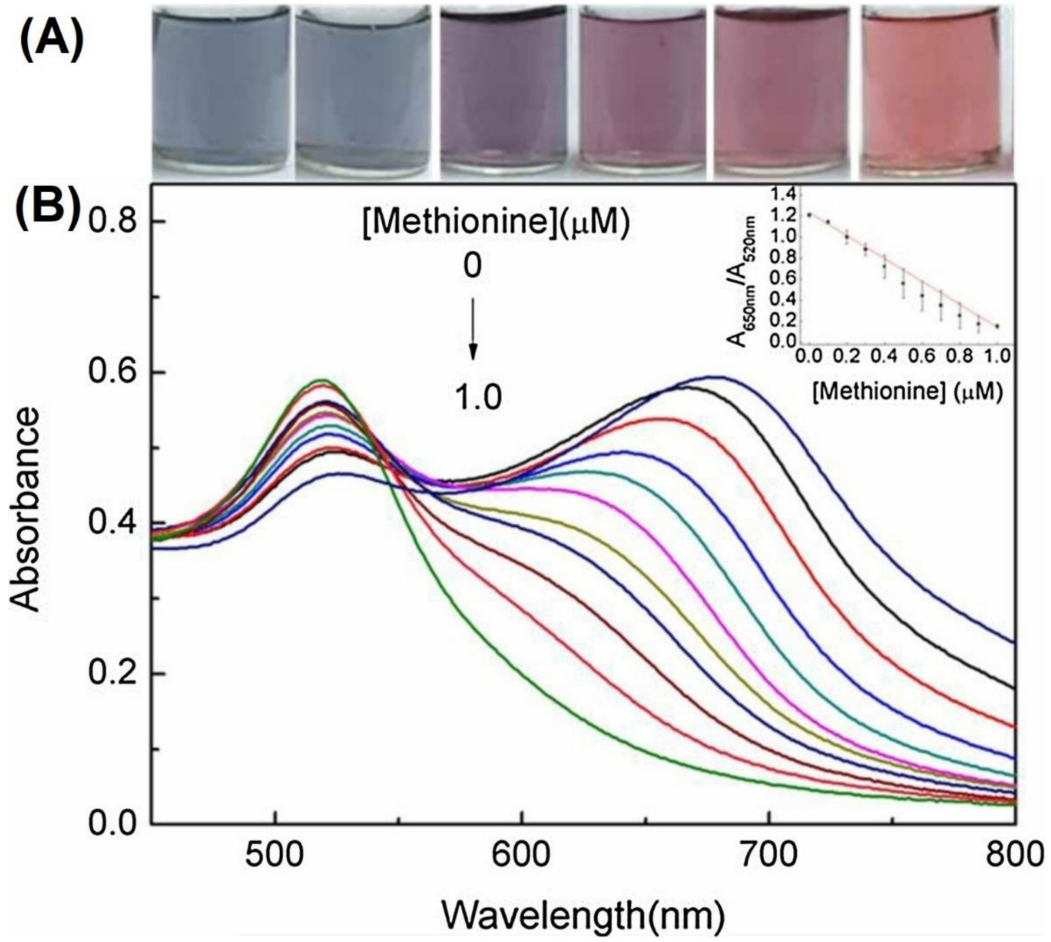

Figure 14. (**A**) Photographic images of the Mel-Au NPs formed in the presence of different concentrations of Met (0, 0.2, 0.4, 0.6, 0.8, and 1.0 μM); (**B**) UV–vis absorption spectra of the Mel-Au NPs generated in the presence of different concentrations of Met (0, 0.1, 0.2, 0.3, 0.4, 0.5, 0.6, 0.7, 0.8, 0.9, and 1.0 μM); inset shows plot of A_{650nm}/A_{520nm} against the Met concentrations ((**A**,**B**) are reproduced with the permission from [82]).

Liu et al. demonstrated the boronic acid–diol binding for a selective colorimetric assay of dihydro-nicotinamide adenine dinucleotide (NADH) [85] in which the CI-Au NPs (particle size = 13 nm; conc. = 3 nM) aggregated in the presence of MPBA (10 μM) via a strong Au-S binding to produce a color change from red to blue. By adding NADH, the

cis-2,3-ribose diol containing sugar units in NADH reacts with boronic acid and induces anti-aggregation with a corresponding color change from blue to red, as seen in Figure 15. To optimize the above pH dependent reaction, a pH value of 10.5 (buffer: 18 mM NaOH from 0.2 M stock) was chosen at a fixed incubation time of 12 min. TEM and SPR studies well attested the anti-aggregation strategy. The linear range of NADH was between 0.008 and 8 μM (at A_{520}/A_{630}), with an LOD of 2 nM. This report is innovative, but it still requires further work in real applications.

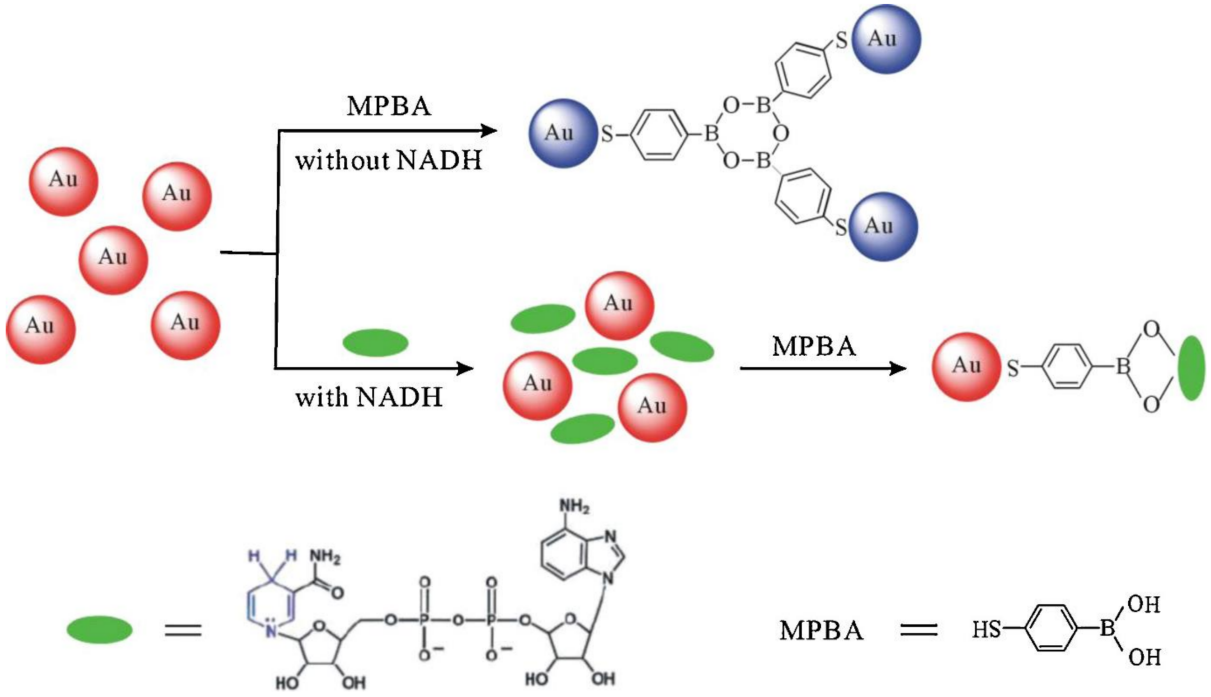

Figure 15. Schematic for colorimetric detection of NADH based on anti-aggregation of Au NPs (reproduced with the permission from [85]).

Sang and co-workers reported anti-aggregation of Au NPs with the support of the aptamer hairpin probe (AHP; 1.5 nM) for colorimetric recognition of adenosine tri-phosphate (ATP) by engaging PDDA (0.5 μM) as the aggregation-inducing agent [86]. In the absence of ATP, PDDA induced aggregation of CI-Au NPs (particle size = 13 nm) due to the strong electrostatic interactions and produced a color change from red to blue. In the presence of ATP, the AHP opened up to expose the flexible single-stranded DNA (ssDNA) to interact with PDDA, which prevented PDDA from inducing Au NPs aggregation and led to a reversed colorimetric response (a color change from blue to red). The optimum incubation time for the experiments was established as 5 min. TEM, DLS, and SPR confirmed the anti-aggregation and colorimetric response to ATP. As shown in Figure 16A,B, ATP shows the SPR linearity as being between 20 and 100 nM (at A_{610}/A_{520}), with an LOD of 1.7 nM. The spiked human serum investigations showed the recoveries of >100%, with an RSD of <3%. Based on the results, this work can be regarded as exceptional for colorimetric assay of ATP. However, the selectivity must be justified by including more competing species.

Zhang et al. discussed the anti-aggregation-enabled colorimetric assay of Y-shaped target DNA (T-DNA) by employing CI-Au NPs (particle size = 30–70 nm) and NaCl (30 mM) as the aggregation-inducing agent [87]. In fact, the non-relevant DNA (in the presence of NaCl) did not affect aggregation of Au NPs and showed a color change from red to royal purple. In contrast, the Y-shaped T-DNA–protected Au NPs did not aggregate in the presence of NaCl, thereby reversing the color from royal purple to red. Both aggregation and dispersion of Au NPs in the presence and absence of T-DNA were authenticated with TEM and DLS interrogations. The best result was attained at pH 3–11 after 5 min

incubation. The SPR linearity was between 5 and 100 nM, with an LOD of 5 nM. The selectivity was confirmed by employing various DNAs. However, real-time colorimetric assays of T-DNA still need more experimental data to confirm feasibility. The sequential colorimetric detection of sanguinarine (SNG; an anti-cancer drug) and Calf Thymus DNA (Ct-DNA) was proposed using CI-Au NPs (particle size = 13 nm; conc. = 0.8 nM) [88]. The SNG (1 μM) was engaged as an aggregation-inducing agent in the presence of 14 mM NaCl and delivered a color change from red to blue at an optimum pH value of 7.4 (buffer: Tris-EDTA (EDTA = Ethylenediamine Tetraacetic acid)) after 10 min incubation. The SNG showed a linearity of between 0 and 0.9 μM (at A_{627}/A_{525}), with an LOD of 46 nM. In contrast, the SNG-induced aggregation of CI-Au NPs is disrupted upon pre-treating with Ct-DNA (in the presence of 14 mM NaCl and at pH 7.4 (Tris-EDTA), after 10 min incubation) due to the strong affinity of SNG to Ct-DNA, thereby reversing the colorimetric response from blue to red/pink, as illustrated in Figure 17. TEM and SPR spectral studies supported the aggregation and anti-aggregation as well as the colorimetric changes. The linear regression of Ct-DNA was between 0 and 5 μM (at A_{525}/A_{627}), with an LOD of 0.36 μM. Both sensory selectivities did not show any interfering effect from the competing species. The colorimetric Ct-DNA assay by this method was validated by human urine analysis, which showed a recovery of >95%, with an RSD of <6%. Thus, it can be noted as a nice innovation toward colorimetric assays of SNG and Ct-DNA.

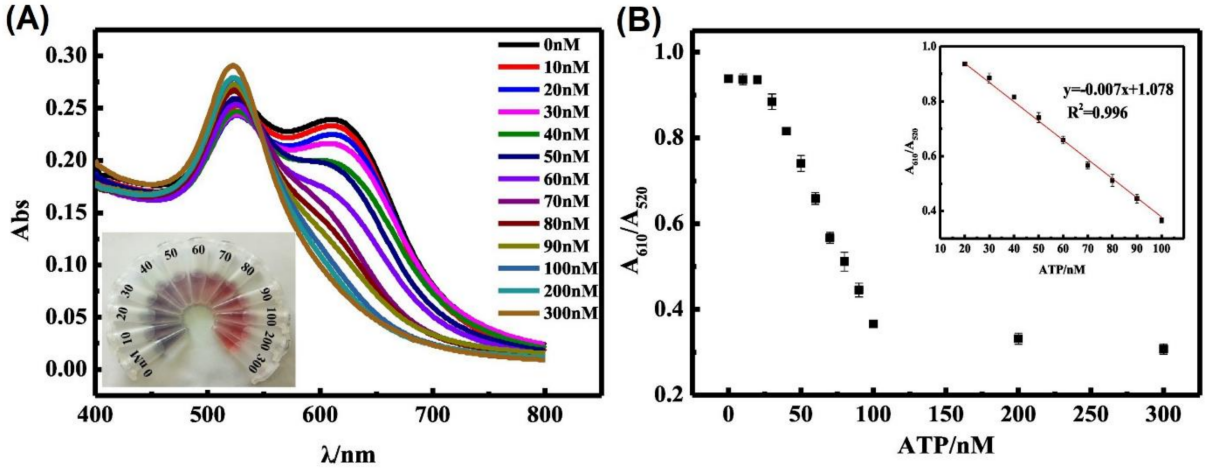

Figure 16. (**A**) UV–vis absorption spectra of the colorimetric assay with various concentrations of ATP (inset: the corresponding photographs of the solutions); (**B**) plot of the absorbance ratio (A_{610}/A_{520}) vs. ATP concentration in the range of 0 to 300 nM. The inset illustrates the linear calibration plot of A_{610}/A_{520} vs. the ATP concentration (20 to 100 nM). Error bars were obtained from three experiments ((**A**,**B**) are reproduced with the permission from [86]).

The anti-aggregation-based colorimetric assay of heparin (an anticoagulant used in the treatment of certain blood vessel, heart, and lung conditions) was proposed by employing 4-mercaptobenzoic acid–stabilized Au NPs (4-MBA-Au NPs; particle size = 41 nm), CI-Au NPs (particle size = 13 nm) modified with protamine (0.6 μg/mL), and PDDA (0.02 μM) as corresponding aggregation agents [89,90]. In both reports, the -vely charged Au NPs interacted with +vely charged protamine and PDDA, which enhanced the aggregation with a colorimetric change from red to blue. Thereafter, pre-mixing of negatively charged heparin with protamine/PDDA led to anti-aggregation of Au NPs (resulted from strong affinity of the +vely charged protamine/PDDA to -vely charged heparin) with a color change from blue to red. The SPR changes of 4-MBA-Au NPs in the presence and absence of protamine and heparin were observed from the relative intensity at 1590 cm^{-1} in Raman spectroscopy investigations (measured at pH 7.4 (buffer: 10 mM HEPES) within few minutes incubation) [89]. The SPR linearity of 4-MBA-Au NPs-protamine to heparin was between 0.05 and 20 ng/mL, with an LOD of 0.03 ng/mL (ng = nanogram; mL = milliliter).

In contrast, CI-Au NPs [90] in the presence of PDDA and heparin (after 3 min incubation) displayed the SPR linearity of between 0 and 0.4 mg/mL (at A_{650}/A_{520}; mg = milligram), with an LOD of 0.02 μg/mL (μg = microgram). TEM studies of both reports confirmed the anti-aggregation-induced by heparin. The real samples investigations (fetal bovine serum and human blood serum, respectively) validated their applicability with recoveries of >90% and an RSD of <6%. These reported are regarded as remarkable inventions on colorimetric assay of heparin; however, further research is mandatory toward commercial applications.

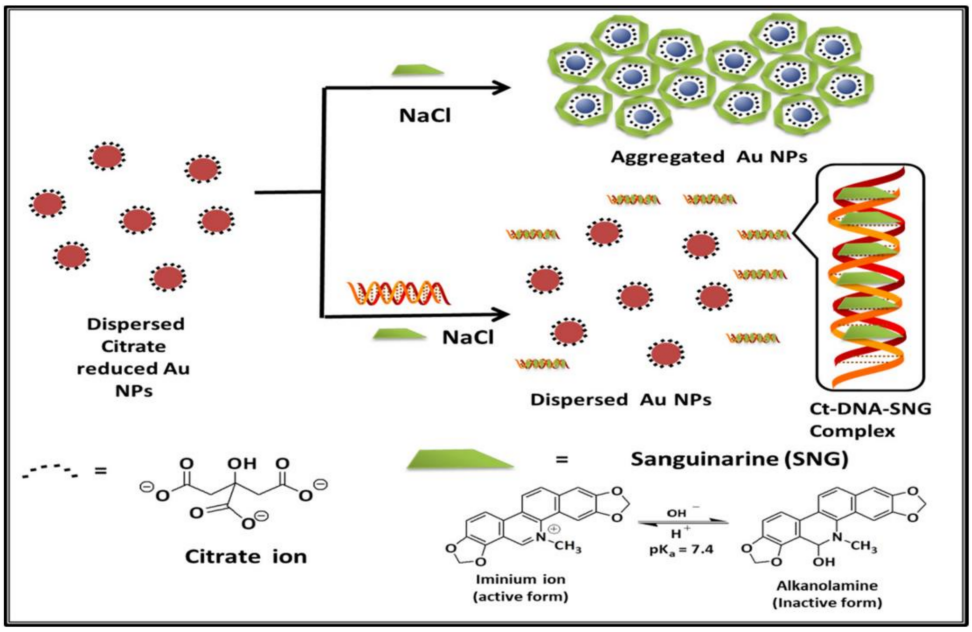

Figure 17. Mechanistic outline for detection of SNG and Ct-DNA using CI-Au NPs as colorimetric probe (reproduced with the permission from [88]).

Kim and co-workers described the anti-aggregation-enabled colorimetric detection and in vitro assay of amyloid β peptide (Aβ; a critical initiator that triggers the progression of Alzheimer's disease (AD) via aggregation) by engaging CI-Au NPs (particle size = 17 nm) in the presence of Cu^{2+} (10 μM; pH 5; 45 °C) [91,92]. These reports provide valuable information on the effects of 10 anti-aggregation agents, such as acetylcholine, albumin, caffeine, catechin, curcumin, glutathione, resveratrol, rutin, silibinin, and trehalose, toward quantification of amyloid β fragments (Aβ (1-40) and Aβ (1-42)) and application in the detection of Alzheimer's disease. In fact, inhibition of Aβ aggregation is essential to avoid the progression of Alzheimer's disease [93]. Thus, they can be regarded as exceptional work based on the anti-aggregation-facilitated colorimetric assay.

The human chorionic gonadotropin (hCG; a hormone produced during pregnancy) and methylglyoxal (MGO; a food toxin) was quantified by anti-aggregation-enabled colorimetric assay [94,95], wherein, CI-Au NPs (particle size = 13 nm) were aggregated in the presence of peptide (0.5 μM) and *o*-phenylenediamine (OPD; 0.5 μM) to display a color change from red to blue. By pre-treating the hCG/MGO with peptide and OPD (at pH 7.4 (buffer: PBS in 18.8 mM NaCl) and at pH 7.5 (buffer: sodium phosphate) after 16 min and 30 min incubation, respectively), the colorimetric response was reversed from blue to red. The underlying mechanism is that the hCG and MGO react with peptide and OPD, respectively, to induce anti-aggregation of Au NPs, which is evident from TEM, DLS, SPR, and interference studies. The HCG showed a linear range of between 50 and 1000 mIU/mL (at A_{600}/A_{525}; mIU = milli-international units), with an LOD of 25 mIU/mL [94]. Likewise, the linearity of MGO was between 0.01 and 10 μM (at A_{520}/A_{680}), with an LOD of 50 nM [95]. Though both works are remarkable, more attention is required in their practicality.

Su et al. proposed the anti-aggregation-enabled colorimetric detection of oxytetracycline (OCT; an antibiotic drug) using cysteamine-stabilized Au NPs (cysteamine-Au NPs)

and aptamer (OBA; 3 nM; sequence: 5′-CGT ACG GAA TTC GCT AGC GGG CGG GGG TGC TGG GGG AAT GGA GTG CTG CGT GCT GCG GGG ATC CGA GCT CCA CGT G-3′) as the aggregation-inducing agent [96]. In the presence of OBA, the cysteamine-Au NPs aggregated with a color change from red to blue, which was re-dispersed (with a color change from blue to red) by OCT via anti-aggregation. In fact, OTC reacted with OBA effectively due to their electrostatic attraction and displayed anti-aggregation, as evident by TEM, DLS, SPR, and interference studies. The linearity of OTC was between 4.34 and 60.81 µM (intensity change at A_{527}), with an LOD of 493 nM. The milk samples analysis showed a recovery of >80%, with an RSD of <3%; thus, it can be included in the OTC quantification tactics.

The anti-aggregation-enabled colorimetric assay of azodicarbonamide (ADA; a flour contaminant) was reported using CI-Au NPs (particle size = 23 nm) and GSH (2.5 µM) as the aggregation-inducing agent [97]. Due to strong electrostatic interaction between Au and SH of CI-Au NPs and GSH, an initial color change occurred (from red to blue) via aggregation. When the above mixture was pre-treated with ADA, oxidation of -SH group (of GSH) by ADA led to the formation of an -S-S-bond; thus, the aggregation was disrupted with a colorimetric response from blue to red. The best result was attained at pH 3.3 (buffer: 3.3 mM BR), 50 °C, and after 60 min incubation. SPR, TEM, and DLS investigations authenticated the anti-aggregation strategy. The linear range of ADA was established as being between 0.12 and 1.00 µM (at A_{520}/A_{668}), with an LOD of 70 nM. This work was also demonstrated in homemade and market flour samples, with recoveries of >90% and an RSD of <6%. Therefore, it can be noted as a remarkable innovation toward flour contaminants detection. Table 3 delivers the linear ranges, LODs, pH (buffer), incubation time, and applications of anti-aggregation-tuned Au NPs-based colorimetric assay of bio-analytes reviewed in this section.

Table 3. Linear ranges, LODs, and applications of Au NPs-based probes reported in anti-aggregation prompted colorimetric detection of bio-analytes.

Probe	Aggregation-Inducing Agent; Optimum Conc.	Sensing Analyte	pH (Buffer); Incubation Time	Linear Range	Limit of Detection (LOD)	Applications	Ref.
CI-Au NPs	S-adenosyl-L-methionine (SAM); 0.8 µM	Glutothione (GSH), cysteine (Cys), and homo-cysteine (HCys)	pH 7 (10 mM BBS); 5 min	0.2–0.9 µM, 0.4–1.2 µM, and 0.6–3.0 µM, respectively	35.8 nM, 21.7 nM, and 62.4 nM, respectively	Biological fluid analysis	[77]
CI-Au NPs	Sodium piperazinebis-dithiocarbamate (ppzdtc); 1.5 µM	Glutothione (GSH)	pH 7.4 (10 mM HEPES); 30 min	8–250 nM	8 nM	NA	[78]
CI-Au NPs	Cysteine (Cys); 4 µM	Glutothione (GSH)	pH 5.8 (PBS); 5 min	0.1–1 µM	20.3 nM	Human urine analysis	[79]
CI-Au NPs	2-Mercapto-1-methylimidazole (MMI); 2 µM	Glutothione (GSH)	pH 5.8 (PBS); 5 min	0.1–1 µM	12 nM	Human serum and urine analysis	[80]
CI-Au NPs	4-mercapto-benzoic acid (4-MBA); 5.2 µM and $CuCl_2$ (400 µM)	D-alanine (D-Ala) in presence of D-amino acid oxidase (DAAO)	pH 7 (HAc-NaAc); 15 min	0.15–30 µM	75 nM	Biological sample analysis	[81]
CI-Au NPs	Melamine (Mel)	Methionine (Met)	pH 7.4 (PBS); 5 min	0–1 µM	24.5 nM	Human serum and urine analysis	[82]
CI-Au NPs	4-Mercaptophenylboronic acid (MPBA); 1.34 µM	Fructose	pH 7 (NA); 10 min	32–960 µM	10 µM	Human plasma analysis	[83]
CI-Au NPs	4-Mercaptophenylboronic acid (MPBA); 10 µM	Dihydro-nicotinamide adenine dinucleotide (NADH)	pH 10.5 (18 mM NaOH); 12 min	0.008–8 µM	2 nM	NA	[85]
CI-Au NPs	Poly-(diallyldimethylammonium chloride) (PDDA); 0.5 µM	adenosine triphosphate (ATP)	NA; 5 min	20–100 nM	1.7 nM	Human serum analysis	[86]
CI-Au NPs	sodium chloride (NaCl); 30 mM	Target Deoxyri-bonucleic Acid (T-DNA)	pH 3–11 (NA); 5 min	5–100 nM	5 nM	NA	[87]

Table 3. *Cont.*

Probe	Aggregation-Inducing Agent; Optimum Conc.	Sensing Analyte	pH (Buffer); Incubation Time	Linear Range	Limit of Detection (LOD)	Applications	Ref.
CI-Au NPs	Sanguinarine (SNG); 1 μM	Calf Thymus DNA (Ct-DNA)	pH 7.4 (Tris-EDTA); 10 min	0–5 μM	0.36 μM	Biological fluid analysis	[88]
4-mercaptobenzoic acid–stabilized Au NPs	Protamine; 0.6 μg/mL	Heparin	pH 7.4 (10 mM HEPES); NA	0.05–20 ng/mL	0.03 ng/mL	Fetal bovine serum analysis	[89]
CI-Au NPs	Poly-(diallyldimethylammonium chloride) (PDDA); 0.02 μM	Heparin	NA; 3 min	0–0.4 mg/mL	0.02 μg/mL	Human blood serum analysis	[90]
CI-Au NPs	Peptide; 0.5 μM	Human chorion-icgonadotropin (HCG)	pH 7.4 (PBS in 18.8 mM NaCl); 16 min	50–1000 mIU/mL	25 mIU/mL	Biological fluid analysis	[94]
CI-Au NPs	*o*-phenylenediamine (OPD); 0.5 μM	Methylglyoxal (MGO)	pH 7.5 (30 mM sodium phosphate); 30 min	0.01–10 μM	0.05 μM	NA	[95]
Cysteamine-stabilized Au NPs	Aptamer (OBA); 3 nM	Oxytetracycline (OTC)	NA; 22 min	4.34–60.81 μM	493 nM	Milk analysis	[96]
CI-Au NPs	Glutothione (GSH); 2.5 μM	Azodicarbonamide (ADA)	pH 3.3 (3.3 mM BR); 60 min	0.12–1.00 μM	70 nM	Flour samples analysis	[97]

NA = Not available; min = minutes; mM = 10^{-3}M; μM = 10^{-6} M; nM = 10^{-9} M; μg = microgram; ng = nanogram; mIU = milli-international units; mL = milliliter.

5. Anti-Aggregation in Au NPs-Based Colorimetric Assay of Pesticides and Herbicides

Liu and co-workers demonstrated the anti-aggregation-enabled colorimetric assay of chlorsulfuron (first sulfonylurea herbicide) by engaging PDDA-Au NPs (particle size = 13 nm) and acetamiprid (an organic compound; 90 μM) as the aggregation-inducing agent [98]. Due to the electrostatic interaction between acetamiprid and PDDA-Au NPs, aggregation occurred with a color change from Bordeaux red to blue. The above reaction was inhibited in the presence of chlorsulfuron because of its strong affinity to acetamiprid, and, hence, the color changed from blue to red due to anti-aggregation of the Au NPs.

The best result was attained at pH 4.5 (buffer: 10 mM NAc-HAc) after 30 min incubation. TEM, SPR, FTIR (FTIR = Fourier transform infrared spectra), and interference studies validated the anti-aggregation, acetamiprid-chlorsulfuron complex, and high selectivity. As seen in Figure 18A,B, the color and SPR spectra show dependence on the chlorsulfuron concentrations (linear range at A_{523}: 0.28–279 μM), with an LOD of 0.14 μM. Tap and well water interrogations showed recoveries of >75%, with an RSD of <8%, but more optimizations are still required toward real applications. Following the similar experimental conditions (pH and incubation time) and mechanistic approach, the anti-aggregation-enabled colorimetric assay of metsulfuron–methyl (a sulfonylurea pesticide) was proposed by employing CI-Au NPs (particle size = 20 nm) and melamine (15.86 μM) as the aggregation-inducing agent [99]. In the presence of melamine, the color of Au NPs changed from red to blue via aggregation. During analyte sensing, the melamine interacted with metsulfuron–methyl via H-bonding, which resulted in anti-aggregation and a reversed color change from blue to red. The linear range of the analyte was between 0.26 and 262 μM (at A_{523}), with an LOD of 131 nM. The real analysis in tap water and well water showed recoveries of >70%, with an RSD of <7%. However, this work requires more effort toward real-time applicability.

Keshvari and co-workers reported the anti-aggregation-enabled colorimetric quantification of catechol (intermediates in pesticides industries) by applying CI-Au NPs and 4-Mercapto-phenyl boronic acid (MPBA; 0.4 μM) as the aggregation-inducing agent [100]. The mercapto (-SH) group in MPBA bound strongly to the Au surface and induced aggregation and a color change from red to blue. However, in the presence of catechol, the Au-S binding was disrupted by the reaction between diol and boronic acid, which resulted in anti-aggregation and a reversed color change (from blue to red). The best result was attained at pH 7.6 after 5 min incubation. The linearity of the catechol detection was between 0.87 and 56 μM (at A_{519}/A_{640}), with an LOD of 0.41 μM. Investigations on river

and plasma samples showed recoveries of >100%. Although TEM and SPR studies reported in this work validated the anti-aggregation, they lacked information of the particle size variations, interference studies with many compounds, and buffer used, thereby requiring more experimental works.

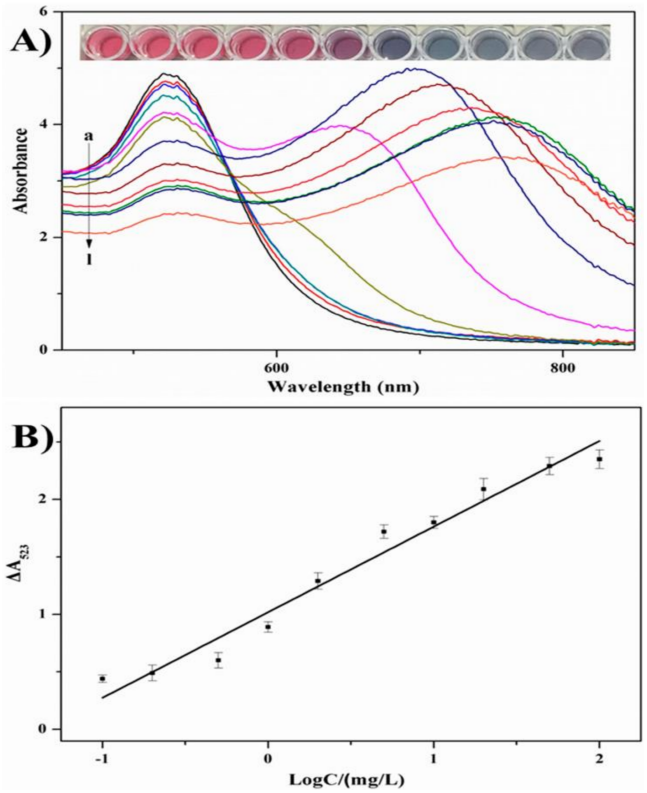

Figure 18. (**A**) UV–vis spectra and a photograph of (a) AuNP solutions and AuNP solutions with concentrations of chlorsulfuron of (b) 100 mg/L, (c) 50 mg/L, (d) 20 mg/L, (e) 10 mg/L, (f) 5.0 mg/L, (g) 2.0 mg/L, (h) 1.0 mg/L, (i) 0.5 mg/L, (j) 0.2 mg/L, (k) 0.1 mg/L, and (l) 0 mg/L in the presence of 20 mg/L acetamiprid and (**B**) standard calibration curve of the absorbance change of Au NPs at 523 nm (ΔA_{523}) against chlorsulfuron concentration ((**A**,**B**) are reproduced with the permission from [98]).

Chen et al. described the distinct colorimetric detection of terbuthylazine (TBA; an herbicide) and dimethoate (DMT; a common organic phosphorus insecticide) by using CI-Au NPs (particle size = 16 nm) via aggregation and anti-aggregation, respectively [101], wherein Au NPs aggregated with a color change from red to blue when 40 mM of NaOH (pH > 9) was added. Pre-mixing of NaOH with DMT induces anti-aggregation, SPR spectral variations (among other interferences), and a color change from blue to red, as visualized in Figure 19A,B. The underlying mechanism is that, during the pre-mixing of NaOH and DMT, a hydrolysis reaction occurred, and the OH^- from NaOH hydrolyzed the methoxy groups (-OCH_3 attached over S-P = S) of DMT to form methanol (CH_3OH), which resulted in the anti-aggregation of Au NPs at an optimum incubation time of 10 min. The linear range of DMT was between 1 and 40 nM (at A_{525}/A_{680}), with an LOD of 6.2 nM. SPR, TEM, DLS, and interference studies well attested the anti-aggregation and DMT selectivity over other competing species. This work was also demonstrated by tap water, green tea, and apple juice analysis with nanomolar LODs. Therefore, based on distinct analyte sensing strategy and real-time applicability, this work can be regarded as an exceptional work.

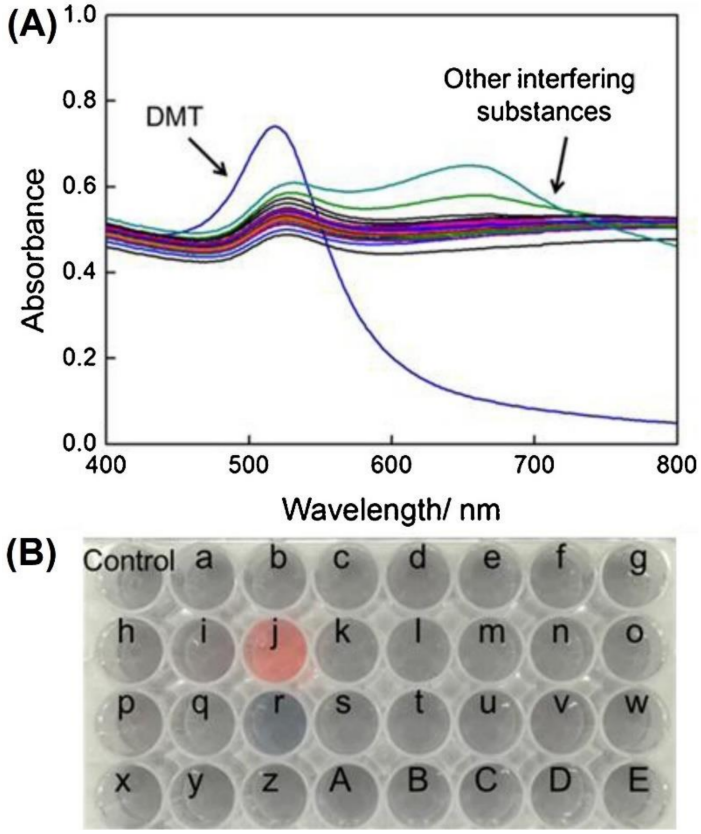

Figure 19. Selectivity of the AuNP-based colorimetric sensor for rapid detection of DMT compared with other substances. UV–vis absorption spectra (**A**) and photographic images (**B**) of the AuNP-based colorimetric sensor (0.86 mL) incubated (10 min) with 40 μL of NaOH (1.0 M) plus 100 μL of DMT (0.2 μM), or plus 100 μL of other substances (1.0 μM), or plus 100 μL of H_2O (control). (a) Iprodione; (b) Dioxacarb; (c) Benzex; (d) Isoprocarb; (e) Chipton; (f) Pretilachlor; (g) Sodium cyclamate; (h): Permethrin; (i) Trichlorphon; (j) Dimethoate; (k) Fenvalerate; (l) Chlorpyrifos; (m) Profenofos; (n) Indoxacarb; (o) Dichlorodiphenyltrichloroethane; (p) Glufosinate-ammonium; (q) Glyphosate; (r) Terbuthylazine; (s) Deltamethrin; (t) D-glucose; (u) Aspartame; (v) K^+; (w) Na^+; (x) Mg^{2+}; (y) Ba^{2+}; (z) Cl^-; (A) NO_3^-; (B) Ac^-; (C) CO_3^{2-}; (D) SO_4^{2-}; (E) PO_4^{3-} (reproduced with the permission from [101]).

By means of base-mediated hydrolysis, anti-aggregation-enabled colorimetric assay of malathion (an organophosphate pesticide) was demonstrated by employing CI-Au NPs (particle size = 13.5 nm, conc. = 7.5 nM) and 40 mM NaOH as the aggregation-inducing agent [102]. In the presence of 40 mM NaOH, Au NPs aggregated with a color change of red to blue. When NaOH was pre-treated with malathion, a hydrolysis reaction occurred to afford methanol (via hydrolysis of -OCH_3 in S-P = S) and ethanol (from hydrolysis of ethyl ester of malathion), which resulted in the anti-aggregation of Au NPs with a color change from blue to red. The best colorimetric response/anti-aggregation was found at pH > 9 (from 40 mM NaOH) and after 20 min incubation. The linear response was between 0.05 and 0.8 μM (at A_{525}/A_{680}), with an LOD of 11.8 nM. This work was validated by TEM, SPR, and real samples (tap water, vegetable, and apple juice) investigations and showed LODs at nM and recoveries of between 94 and 107%, with an RSD of <8%. However, interference studies must be improved by including more competing species.

Chungchai et al. described the anti-aggregation-based colorimetric detection of chlorpyrifos (an organophosphate pesticide) by engaging graphene-quantum-dot–capped gold nanocomposite particles (GQD-Au NPs; particle size = 12 ± 0.26 nm) [103]. Herein, acetylthio-choline chloride (ATCh; 50 μM) was utilized as an aggregation-inducing agent in the presence of acetylcholinesterase (AChE). The AChE reacted with ATCh to produce

thiocholine, which caused the aggregation of GQD-Au NPs with a color change from red to blue-purple. The above reaction was inhibited in the presence of chlorpyrifos; therefore, production of thiocholine was inhibited, which resulted in anti-aggregation and a color change from blue-purple to red. The best result was attained at pH 7 (buffer: PBS) after 15 min incubation. The linear range of chlorpyrifos was between 0.29 and 143 μM (at A_{520}), with an LOD of 131 nM. This work was attested by SPR, TEM, interference, vegetable sample, and microfluidic paper-based analytical device (3D-μPAD) studies. Therefore, it can be regarded as a nice innovation but still requires careful optimizations on the concentrations of AChE and ATCh.

Liu et al. employed the 4-aminothiophenol (4-ABT)-functionalized Au NPs (Au NPs@4-ABT; particle size = 63 ± 6 nm) toward anti-aggregation-facilitated colorimetric detection of thiram (a protective fungicide for the storage and shipment of fruit, grain, and vegetable) using Ag^+ (1 μM) as the aggregation-inducing agent [104]. As seen in Figure 20, Au NPs@4-ABT aggregate in the presence of Ag^+ (via strong binding between free -NH_2 and Ag^+) to deliver a color change from red to blue. However, when thiram is pre-mixed with Ag^+, the reaction between Au NPs@4-ABT to Ag^+ is inhibited (due to a strong affinity between thiram and Ag^+), which results in anti-aggregation with a color change from blue to red, as displayed in Figure 20. The best colorimetric response was obtained at pH 7.5 (buffer: 10 mM PBS) after 12 min incubation. The linear range of thiram was between 0.05 and 2.0 μM (at A_{542}), with an LOD of 40 nM. TEM, SPR, XPS, DLS, interference, and real samples (apple and soil; recoveries of >80%, with an RSD of <5%) studies validated the proposed colorimetric method toward thiram quantification. Thus, it can be regarded as an outstanding research in food contaminant detection.

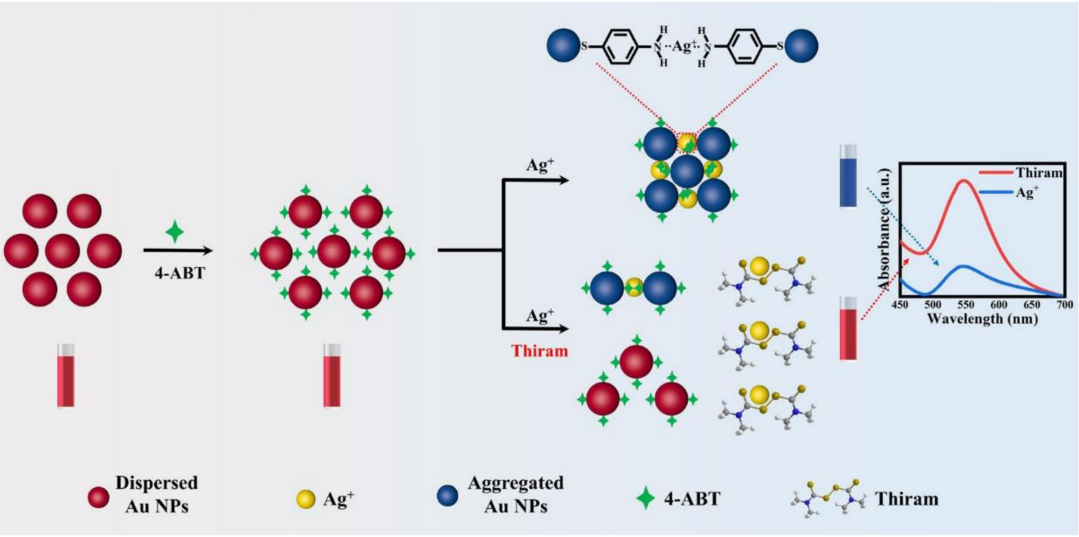

Figure 20. The schematic illustration for thiram detection via Au NPs@4-ABT probe (reproduced with the permission from [104]).

Subsequently, the use of CI-Au NPs (particle size ≥ 10 nm) for anti-aggregation-enabled colorimetric detection of glyphosate (GPS, an herbicide) was reported in the presence of Pb^{2+} (35 μM; aggregation-inducing agent) [105], wherein Pb^{2+} induced aggregation of Au NPs and displayed a color change from wine-red to gray. The pre-mixing of GPS with Au NPs hindered the aggregation process and led to a reversed colorimetric response with a color change from gray to red. The best response was achieved at pH 7 after 10 min incubation. The GPS showed the linearity of between 0 and 0.8 μM (at A_{520}/A_{680}), with an LOD of 2.38 nM. This work is exceptional as demonstrated in TEM, DLS, competing analysis (with 13 interferences), and real water (tap and lake water; recoveries of ≥90%) investigations. Table 4 summarizes information on the linear ranges, LODs, pH (buffer), incubation time, and applications of Au NPs-based probes reported in anti-aggregation-facilitated colorimetric detection of pesticides and herbicides.

Table 4. Linear ranges, LODs, pH (buffer, incubation time and applications of Au NPs-based probes reported in anti-aggregation-facilitated colorimetric detection of pesticides and herbicides.

Probe	Aggregation-Inducing Agent; Optimum Conc.	Sensing Analyte	pH (Buffer); Incubation Time	Linear Range	Limit of Detection (LOD)	Applications	Ref.
PDDA-Au NPs	Acetamiprid; 90 μM	Chlorsulfuron	pH 4.5 (10 mM NAc-HAc); 30 min	0.28–279 μM	0.14 μM	Real water analysis	[98]
CI-Au NPs	Melamine; 15.86 μM	Metsulfuron-methyl	pH 4.5 (10 mM NAc-HAc); 30 min	0.26–262 μM	131 nM	Real water analysis	[99]
CI-Au NPs	4-Mercapto-phenyl boronic acid (MPBA); 0.4 μM	Catechol	pH 7.6 (NA); 5 min	0.87–56 μM	0.41 μM	Real water analysis	[100]
CI-Au NPs	40 mM NaOH	Dimethoate (DMT)	pH > 9 (40 mM NaOH); 10 min	1–40 nM	6.2 nM	Real water, tea, and apple juice analysis	[101]
CI-Au NPs	40 mM NaOH	Malathion	pH > 9 (40 mM NaOH); 20 min	0.05–0.8 μM	11.8 nM	Real water, vegetable and apple juice analysis	[102]
GQDs-Au NPs	Acetylthio-choline chloride (ATCh); 50 μM in presence of Acetylcholinesterase (AChE)	Chlorpyrifos	pH 7 (PBS); 15 min	0.29–143 μM	131 nM	Vegetable analysis	[103]
Au NPs@4-ABT	Ag^{+}; 1 μM	Thiram	pH 7.5 (10 mM PBS); 12 min	0.05–2.0 μM	40 nM	Apple and soil analysis	[104]
CI-Au NPs	Pb^{2+}; 35 μM	Gly-phosate (GPS)	pH 7 (NA); 10 min	0–0.8 μM	2.38 nM	Real water analysis	[105]

NA = Not available; min = minutes; mM = 10^{-3} M; μM = 10^{-6} M; nM = 10^{-9} M.

6. Ag NPs-Based Colorimetric Assay of Diverse Analytes via Anti-Aggregation

Silver nanoparticles (Ag NPs) were also reported toward distinct analyte quantification via the anti-aggregation strategy similar to Au NPs, as discussed in this section. Duan et al. described the use of citrate-capped Ag NPs (CI-Ag NPs) toward the detection of Hg^{2+} via anti-aggregation in the presence of the aggregation-inducing agent 6-thioguanine (0.83 μM) [106], in which 6-thioguanine induced aggregation of Ag NPs to produce a color change from yellow to brown. However, the brown color was reversed to yellow via anti-aggregation by pre-mixing Hg^{2+} (at different concentrations). The underlying mechanism was that 6-thioguanine induced aggregation due to its strong electrostatic interaction toward CI-Ag NPs. However, the aggregation was inhibited by the presence of Hg^{2+} (via strong binding of 6-thioguanine with Hg^{2+}) and resulted in the anti-aggregation of CI-Ag NPs. The best colorimetric response was achieved at pH 4 (100 mM HAc-NaAc) after 30 min incubation. The linear range of Hg^{2+} was between 0 and 333 nM (at A_{530}/A_{394}), with an LOD of 4 nM. SPR, TEM, interference, and spring water studies (recoveries of between 103 and 105%) validated this work as a major innovation. Figure 21A–C display the colorimetric response, SPR variations, and linearity of Hg^{2+} induced anti-aggregation of 6-thioguanine-CI-Ag NPs system, respectively.

Anti-aggregation-enabled colorimetric assay of Cu^{2+} was demonstrated by employing CI-Ag NPs and engaging 1,4-dithiothreitol (DTT; 10 μM) as the aggregation-inducing agent [107], wherein DTT induced the aggregation of Ag NPs via a strong Ag-S bonding and displayed a color change from yellow to deep green. Upon pre-mixing Cu^{2+} in 2,6-pyridinedicarboxylic acid (PDCA, 5 mM), the DTT oxidized to form an intramolecular-S-S-bond, which inhibited aggregation and produced a reversed color change from deep green to yellow. The best result was attained at pH 2–10 (buffer: HCl-NaOH) after 20 min incubation. The linearity of Cu^{2+} was between 0.1 and 2 μM (at A_{408}), with an LOD of 0.1 μM. SPR, TEM, interference, and real samples (tap water and ground water; recoveries of ≥95%, with an RSD of <8%) interrogations validated this method. Hence, it can be regarded as a remarkable research, but details on particle size variations are still missing.

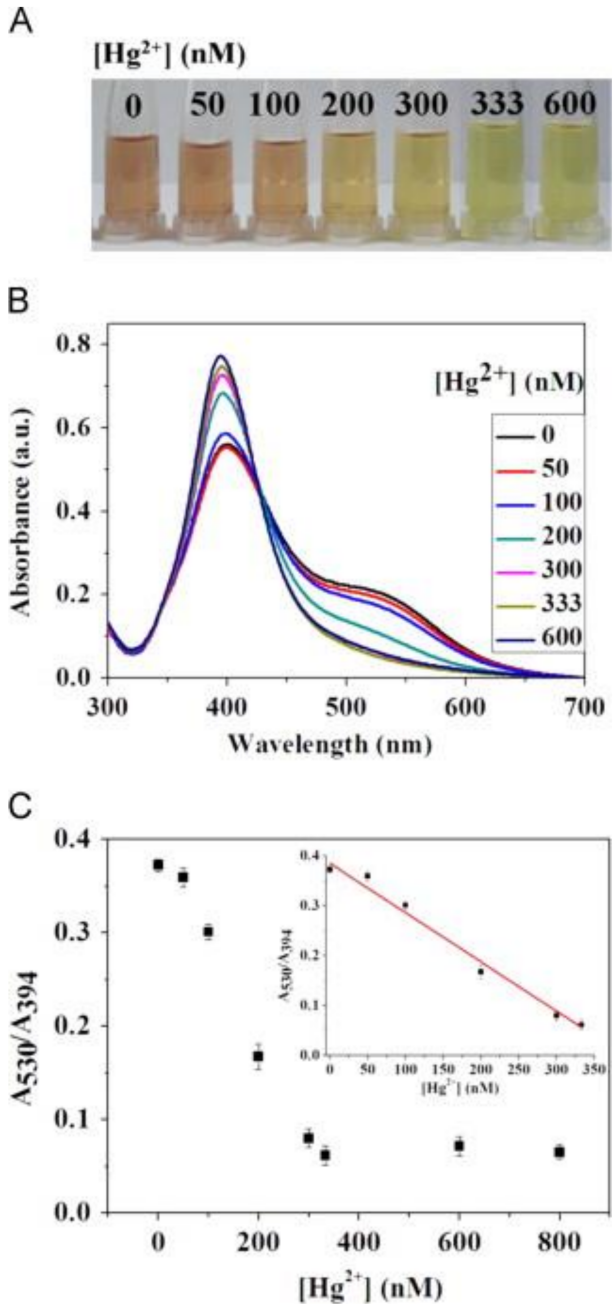

Figure 21. (**A**) The photographic images of the 6-thioguanine–Ag NPs solutions in the presence of different concentrations of Hg^{2+} (0–600 nM). (**B**) The corresponding UV–vis spectra of 6-thioguanine–Ag NPs. (**C**) The absorbance ratio (A_{530}/A_{394}) of 6-thioguanine–Ag NPs versus Hg^{2+} concentration. Inset to C: plot of A_{530}/A_{394} versus the Hg^{2+} concentration. The concentration of 6-thioguanine was 0.83 μM ((**A**–**C**) are reproduced with the permission from [106]).

He and co-workers reported the anti-aggregation-enabled colorimetric detection of Mn^{2+} by employing CI-Ag NPs (conc. = 0.28 nM) and L-Arginine (L-Arg; 0.7 mM) as the aggregation-inducing agent [108]. The Ag-N covalent interaction between Ag NPs and L-Arg caused aggregation, with the color of the solution changing from yellow to colorless. The color of Ag NPs changed back from colorless to yellow via anti-aggregation when the above solution was pre-treated with different concentrations of Mn^{2+}. In fact, the anti-aggregation was attributed to the stronger attraction of L-Arg toward Mn^{2+} than that of the Ag NPs. The best result was obtained at pH 9.4 (buffer; BR) after 40 min incubation. Two linear ranges for Mn^{2+} were established between 0 and 700 nM and 5 and 70 μM (both

at A_{390}), with an LOD of 20 nM. As illustrated in Figure 22A,B, none of the competing species shows interference to Mn^{2+} selectivity. By this method, real water (lake, tap, and river) recoveries were >90%, with an RSD < 3%. This work is regarded as an exceptional innovation, but it still lacks particle size variations details.

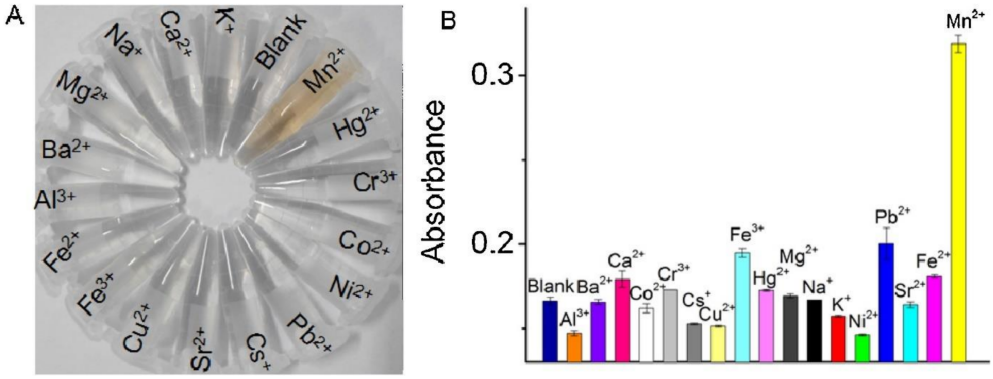

Figure 22. (**A**) The photographs and (**B**) the corresponding absorbance of the Ag NPs-l-arginine dispersions in the presence of different metal ions. The concentrations of both Mn^{2+} ions and other metal ions were 10 μM ((**A**,**B**) are reproduced with the permission from [108]).

Basiri et al. developed the Ag NPs–decorated graphene nanocomposites (rGO@Ag NPs; particle size = 3.7 ± 0.8 nm) for anti-aggregation-enabled colorimetric detection of Cu^{2+} using dopamine (DA; 25 μM) as the aggregation-inducing agent. The Ag NPs and 5 mg/mL of rGO was boiled at pH 10 and at 100 °C for 10 min to afford rGO@Ag NPs. The rGO@Ag NPs were well characterized by SPR, TEM, FTIR, XPS, and XRD studies (XRD = X-ray diffraction). Due to the H-bonding and π–π interactions between DA and rGO@Ag NPs, aggregation occurred (witnessed by TEM) with a color change from yellow to brown. In the presence of Cu^{2+}, the interaction of DA to rGO@Ag NPs was hindered due to selective chelation of Cu^{2+} with DA and resulted in anti-aggregation (seen by TEM) with a color change from brown to yellow. Note that none of the competing species induces anti-aggregation, as shown in Figure 23. The best colorimetric response was observed at pH 7 (buffer: 10 mM PBS) after 15 min incubation. The linearity of Cu^{2+} ranged between 0.02 and 1.5 μM (at A_{405}/A_{515}), with an LOD of 9.8 nM. Moreover, real samples (human urine for DA and tomato for Cu^{2+}) investigations demonstrated recoveries of >98%, with an RSD of <3%; thus, it can be noted as an excellent method.

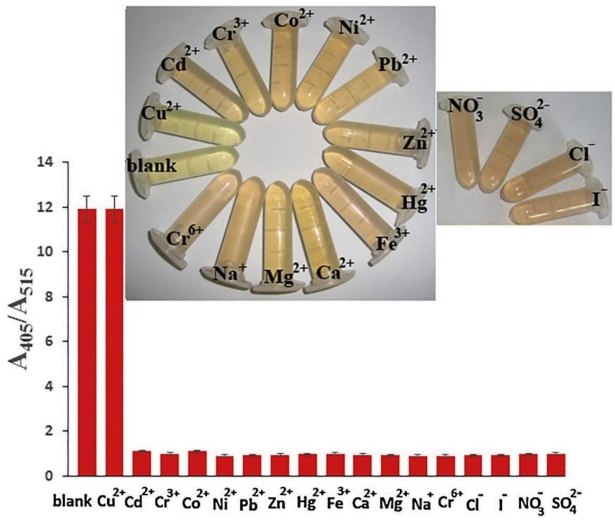

Figure 23. Colorimetric signals in the presence of different metal ions and anions (1.5 μM) as the interferences of Cu^{2+}. Inset: the photographic images of the corresponding solutions (reproduced with the permission from [109]).

An anti-aggregation-enabled colorimetric assay of Br^- and I^- was demonstrated using CI-Ag NPs (particle size = 10–15 nm; conc. = 69.4 μM) and Cr^{3+} (125 μM) as the aggregation-inducing agent [110]. In the presence of Cr^{3+}, the Ag NPs aggregated to produce a color change from yellow to brown. Due to the complexation of Cr^{3+} with Br^- and I^-, anti-aggregation occurred to reverse the color from brown to yellow. The linearity of Br^- and I^- was between 0.99 and 5.66 μM (at A_{500}) and 0.99 and 4.16 μM (at A_{500}), with LODs of 1.67 μM and 1.32 μM, respectively. Though this report was validated by SPR, DLS, and interference studies, data in TEM, pH, incubation time, and real-time investigations were insufficient; therefore, it can be only regarded as a preliminary work. To this track, the sulfanilic acid (SA) and catechol (CAT)–functionalized Ag NPs aggregate (SA-CAT-Ag NPs) was utilized for anti-aggregation-enabled colorimetric detection of F^- [111]. The CA was firstly oxidized by silver ions followed by SA nucleophilic attack to deliver aggregated SA-CAT-Ag NPs with red color. By adding F^- to the above mixture, it adsorbed on the Ag surface and stripped the SA-CAT stabilizer from -$SO_3{}^-$ moiety, hence the aggregation was disturbed with a color change from red to yellow. The best color response was attained at pH 4–9 after 1 min incubation. The linear range of F^- was between 1 and 40 μM (at A_{397}/A_{508}), with an LOD of 0.2 μM. This work was authenticated by SPR, TEM, interference (negligible), and spring water investigations. Thus, it can be noted as a nice approach for F^- quantification.

Dong et al. demonstrated using poly-vinyl pyridine (PVP)–modified Ag NPs (PVP-Ag NPs; particle size = 6.24 nm) the colorimetric assay pyrophosphate (($P_2O_7{}^{4-}$; PPi) via the anti-aggregation strategy [112]. Herein, the Pb^{2+} (5 μM) was employed as the aggregation-inducing agent to induce the PVP-Ag NPs (due to its crosslink effect with PVP) aggregation and to produce a color change from yellow to blue. Anti-aggregation was induced by pre-mixing PPi, which resulted in a colorimetric response from blue to yellow due to the chelating interaction between PPi and Pb^{2+}. The best result was obtained at pH 5–9 at 20 °C after 30 min incubation. The linear ranges of PPi were between 0.2 and 2.0 μM and 2.0 and 10.0 μM (at A_{396}), with an LOD of 0.2 μM. This work was authorized by smartphone device, SPR, TEM, statistical, theoretical, interference, real samples (tap water (recoveries between 79.6 and 107.6%) and canned meat (66.7–118.4%)) interrogations. Therefore, it can be regarded as an exceptional invention in Ag NPs-based colorimetric assay. Following a similar mechanistic approach, the 2-Mercapto-ethane sulfonate–modified silver nanoplates (MS-Ag NPls) were employed in the colorimetric detection of $PO_4{}^{3-}$ (Pi) on PADs in the presence of the aggregation-inducing agent Eu^{3+} (65.81 μM) [113]. In the presence of Eu^{3+}, the color of MS-Ag NPls changed from pink to purple, which was reversed (from purple to pink) during the quantification of Pi. All the sensory experiments were conducted at pH 7 (buffer: 25 mM Tris) at an optimum incubation time of 3 min. The linear regression of Pi was between 10.42 and 313 μM (at A_{520}), with an LOD of 3.44 μM. This work was also authenticated by water and soil investigations. Moreover, this is the only report available on the Ag NPls-based colorimetric assay. Therefore, it is regarded as a remarkable method.

The surface-enhanced Raman scattering (SERS) technique was employed with 4-mercaptopyridine (4-MPY)-modified Ag NPs (4-MPY-Ag NPs) for anti-aggregation-enabled detection of trypsin (an enzyme that aids with digestion) in the presence of the aggregation-inducing agent protamine (0.3 μg/mL (10 μL)) [114]. The presence of +vely charged protamine over 4-MPY-Ag NPs induced aggregation via strong electrostatic interaction with a color change from yellow to deep green. However, trypsin enhanced the enzymatic fragmentation of protamine, which resulted in anti-aggregation with a reversed color change from deep green to yellow. The SERS linear range was between 0.14 nM and 13.8 μM (at 1096 cm^{-1}), with an LOD of 0.14 nM. All the SERS experiments were conducted at pH 7.4 (buffer: HEPES) within 1 min. Based on SERS, TEM, and interference studies, this work can be regarded as a unique one. An anti-aggregation-enabled colorimetric assay of poly diallyl-dimemethyl-ammonium chloride (PDADMAC; a coagulant in water and wastewater treatment) was proposed by employing CI-Ag NPs (particle size = 6 ± 2 nm) and 0.2 M PBS buffer (pH 7.4) as the aggregation-inducing agent [115]. The phosphate

buffer induced aggregation of Ag NPs, which resulted in a color change from yellow to colorless. However, in the presence of PDADMAC, the Ag NPs were stabilized by electrostatic attraction and steric hindrance, which resulted in being dispersed NPs with a reversed color change (from colorless to yellow). Note that the colorimetric responses occurred within 3 min. The linear range of PDADMAC was between 1 and 100 mg. L^{-1} (at A_{396}), with an LOD of 0.7 mg. L^{-1}. This tactic was well authorized by SPR, TEM, interference, and tap water interrogations. Thus, it can be noted as a nice innovation. However, further optimization is mandatory toward the LOD reduction. Table 5 summarizes the linear range, LODs, pH (buffer), incubation time, and applications of Ag NPs-based probes reported in anti-aggregation-facilitated colorimetric detection of various analytes.

Table 5. Linear ranges, LODs, pH (buffer), incubation time, and applications of Ag NPs-based probes reported in anti-aggregation-facilitated colorimetric detection of various analytes.

Probe	Aggregation-Inducing Agent; Optimum Conc.	Sensing Analyte	pH (Buffer); Incubation Time	Linear Range	Limit of Detection (LOD)	Applications	Ref.
CI-Ag NPs	6-Thioguanine; 0.83 μM	Hg^{2+}	pH 4 (100 mM HAc-NaAc); 30 min	0–333 nM	4 nM	Real water analysis	[106]
CI-Ag NPs	1,4-Dithiothreitol (DTT); 10 μM	Cu^{2+}	pH 2–10 (HCl-NaOH); 20 min	0.1–2 μM	0.1 μM	Real water analysis	[107]
CI-Ag NPs	L-Arginine (L-Arg); 0.7 mM	Mn^{2+}	pH 9.4 (BR); 40 min	0–700 nM and 5–70 μM	20 nM	Real water analysis	[108]
rGO@Ag NPs	Dopamine (DA); 25 μM	Cu^{2+}	pH 7 (10 mM PBS); 15 min	0.02–1.5 μM	9.8 nM	Human urine and tomato samples analysis	[109]
CI-Ag NPs	Cr^{3+}: 125 μM	Br^- and I^-	NA	0.99–5.66 μM (Br^-), 0.99–4.16 μM (I^-), respectively	1.67 μM (Br^-) and 1.32 μM (I^-), respectively	NA	[110]
SA-CAT-Ag NPs	Sulfanilic acid and catechol	F^-	pH 4–9 (NA); >1 min	1–40 μM	0.2 μM	Real water analysis	[111]
PVP-Ag NPs	Pb^{2+}; 5 μM	Pyrophosphate ($P_2O_7^{4-}$; PPi)	pH 5–9 (NA); 30 min	0.2–2.0 μM and 2.0–10.0 μM	0.2 μM	Real water analysis	[112]
2-Mercapto-ethane sulfonate–modified silver nanoplates (MS-AgNPls)	Eu^{3+}; 65.81 μM	PO_4^{3-} (Pi) on PADs	pH 7 (25 mM Tris); 3 min	10.42–313 μM	3.44 μM	Real water and soil analysis	[113]
4-MPY-Ag NPs	Protamine; 0.3 μg/mL	Trypsin	pH 7.4 (10 mM HEPES); <1 min	0.14 nM–13.8 μM	0.14 nM	NA	[114]
CI-Ag NPs	0.2 M Phosphate buffer	Poly (diallyl-dimemethyl-ammonium chloride) (PDADMAC)	pH 7.4 (0.2 M PBS); 3 min	1–100 mg. L^{-1}	0.7 mg. L^{-1}	Real water analysis	[115]

NA = Not available; mM = 10^{-3} M; min = minutes; μM = 10^{-6} M; nM = 10^{-9} M; mg = milligram; μg = microgram.

Though anti-aggregation-enabled Ag NPs-based colorimetric assays seem to be effective in analytes quantification, available reports are much less sufficient than that of aggregated Ag NPs-based colorimetric sensors [116–121]. Therefore, further research is required as suggested in perspectives.

7. Design/Sensory Requirements, Advantages, and Limitations

7.1. Probe Design and Sensory Requirements

The development of exceptional Au NPs- and Ag NPs-based colorimetric probes and their anti-aggregation-enabled sensory performances must follow the requirements as stated below:

1. The selected label-free/modified Au NPs- or Ag NPs-based probes must possess dispersion stability in color and firm electrostatic charges to be able to interact with aggregation-inducing agents and to afford a certain degree of aggregation and a distinct colorimetric response.
2. Selection of a suitable aggregation-inducing agent is essential to attain the primary colorimetric changes. An aggregation-inducing agent should have any of the following three characteristics: (i) analyte replaceable electrostatic interactions, (ii) analyte disposable interactive binding (such as Au-S, Ag-S, Au-N, Ag-N, etc.) over the NPs' surface, and (iii) analyte coordinative units (such as thymine, -SH, -NH_2, -COOH, -OCH_3, and -OC_2H_5, etc.) that are able to form coordination complexes or undergo catalytic reactions to be released from the NPs' surface. Moreover, it is essential to fix the concentration of the aggregation-inducing agent before taking further sensory interrogations.
3. Optimizations of the effective pH conditions, suitable pH buffer solution, concentration, and maintenance circumstances are necessary for anti-aggregation-based colorimetric analyte detection.
4. It is essential to fix the exact incubation time to achieve stable colorimetric response and to help to clarify the underlying mechanism and kinetics of the anti-aggregation.
5. Though most of the anti-aggregation-enabled colorimetric sensory are conducted at room temperature, it is also important to fix the operative temperature toward real-time applications.
6. To avoid complications in real water investigations, it is necessary to identify the interfering effect, allowed concentration, required masking agent, etc.

7.2. Advantages

Anti-aggregation-enabled Au NPs- and Ag NPs-based colorimetric assays have following advantages, as stated below:

1. In general, anti-aggregation-enabled Au NPs- and Ag NPs-based analyte quantifications are conducted in an aqueous environment; therefore, they are tactics comparable to the available luminescent inorganic and organic nanomaterials-based sensors performed in diverse solvent conditions [122–130].
2. The anti-aggregation-enabled Au NPs- and Ag NPs-based analyte detection can be observed with naked eye, thereby becoming a competing strategy to the reported organic dyes-based sensors [131–137].
3. In the anti-aggregation-enabled sensory studies, sequential colorimetric detection of the aggregation-inducing agent and analyte can be carried out with reliable linearity and LODs down to nano- and pico-molar levels. Thus, it can be regarded as an advantage over other methods.
4. By using the anti-aggregation-enabled Au NPs- and Ag NPs-based colorimetric assay, diverse analytes can be detected with specificity under a fixed pH value, incubation time, and operative temperature.
5. Anti-aggregation of Au NPs in the presence of certain peptide sequences can be employed to avoid amyloid β aggregation and Alzheimer's disease occurrence.
6. The anti-aggregation strategy in Au NPs- and Ag NPs-based colorimetric sensors can be effectively applied in real samples, such as water, soil, plasma, urine, etc.; thus, it can be noted as a great advantage toward development of the "state of the art" method.

7.3. Limitations

Anti-aggregation-enabled Au NPs- and Ag NPs-based colorimetric sensors also have a few limitations, as discussed below:

1. Anti-aggregation-enabled Au NPs- and Ag NPs-based colorimetric sensory responses are aquatic environment-dependent; therefore, the detection of analytes in other solvent systems is not possible with this method.
2. There are many optimization conditions (such as the aggregation-inducing agent, pH (buffer), NaCl effect, incubation time, temperature, etc.) required in order to attain the sensory responses, thereby limiting the frequent use of the anti-aggregation strategy.
3. Due to the co-existence of the aggregation-inducing agent and analyte in the same mixture, the re-use of the mixture is not possible at all. Similarly, many reports used complicated assay protocols, which may have led to unknown human errors and restricted the use of this method.
4. Elucidation of precise sensory mechanisms requires supportive evidence, such as FTIR, TEM, XPS, XRD, etc. Thus, this method was limited by available instruments and cost-effectiveness.
5. The best result of anti-aggregation-enabled Au NPs- and Ag NPs-based colorimetric sensors can only be attained at a fixed interfering specie concentration, which is not possible with real samples (may contain large amounts of interference); therefore, real-time use of the strategy is still questionable.
6. Real water/soil samples from different places contain various complicated matrixes. Thus, applying the anti-aggregation-enabled Au NPs- and Ag NPs-based colorimetric assay to all the real samples is not possible or may not deliver expected results.

8. Conclusions and Perspectives

In this review, discussions on anti-aggregation-enabled Au NPs- and Ag NPs-based colorimetric sensing of metal ions, anions, bio-analytes, pesticides, and herbicides are delivered in great details. The assay protocols, optimized concentrations of aggregation-inducing agents, pH (buffer solution), incubation times, and operating temperatures are provided and tabulated for readers. The exact underlying mechanisms of each probe leading to the colorimetric response are explained with clear evidence. Real-time applications are illustrated, and comments are given on the performance of each individual report. Finally, we suggest the probe design/sensory requirements together with the merits and limitations of the anti-aggregation strategy. Though the anti-aggregation strategy-based colorimetric sensors are noted as being great innovations, there are still a few perspective points that need to be focused on, as noted below:

1. Most reports on anti-aggregation-enabled Au NPs- and Ag NPs-based colorimetric sensors used complicated assay protocols, which should be simplified toward "state of the art".
2. Performance of anti-aggregation-enabled Au NPs- and Ag NPs-based colorimetric sensors depends on the pH values and buffer used. The use of unified pH buffer solution must be justified in the future to achieve a unique anti-aggregation strategy.
3. By means of anti-aggregation, numerous reports are available on Au NPs-based colorimetric assay of Hg^{2+}; however, none of them were commercialized toward practicality. This requires more efforts in future.
4. The majority of anti-aggregation-based colorimetric sensors by Au NPs and Ag NPs focused on single-analyte quantification so far, which must be upgraded to multi-analyte detection. For example, the aggregation-inducing agent Hg^{2+} also has the coordination tendency for biothiols and I^{-}, hence it can be employed in the quantification of both analytes.
5. In many reports, anti-aggregation due to coordination of aggregation agents with analytes was not supported by valid evidence, which requires further clarification.

6. Currently, anti-aggregation-enabled Au NPs- and Ag NPs-based colorimetric sensors are only available for the detection of limited metal analytes (such as Hg^{2+}, Cu^{2+}, Ag^{+}, Mn^{2+}, and Sc^{3+}), thereby requiring more attention toward developing discrimination of more metal ion species.
7. Anti-aggregation proposed for oxidative catalytic reactions falls short of evidence, and it should be addressed with more experimental data.
8. Concerning the social impact, anti-aggregation-enabled in vitro colorimetric assay of amyloid β peptide toward the inhibition of Alzheimer disease requires great attention in future research work.
9. Reports on anti-aggregation-enabled Au-NPs colorimetric assay of anions, pesticides, and herbicides are insufficient to justify the effectiveness of the strategy toward those analytes. This issue should be addressed in future.
10. Only a few reports are available on the anti-aggregation-stimulated Ag NPs-based colorimetric sensors toward diverse analytes detection. Therefore, research on anti-aggregation of Ag NPs toward the discrimination of distinct analytes requires great attention.
11. Compositions of Au NPs and Ag NPs with other established luminescent nanomaterials can be the focus to afford anti-aggregation-based colorimetric and luminescent responses toward specific analytes.
12. Many anti-aggregation-based sensory reports lack theoretical supports, which should be addressed using density functional theory (DFT) investigations in future.

Though there are still many unclearly issues requiring further clarification, colorimetric recognition of specified analytes via anti-aggregation is becoming an important research field. Currently, there are many groups working on the development of new anti-aggregation-enabled Au NPs- and Ag NPs-based colorimetric sensory probes to remedy the aforementioned issues. However, the anti-aggregation strategy can be regarded as exceptional for analyte quantification in terms of naked eye detection ability and real-time applicability.

Author Contributions: Literature collection, M.S.: Writing—original draft preparation, M.S.; writing—review and editing, K.-W.S.; supervision, K.-W.S.; project administration, K.-W.S.; funding acquisition, K.-W.S. All authors have read and agreed to the published version of the manuscript.

Funding: This research was funded by the Ministry of Science and Technology of Taiwan under the contract No. MOST 111-2112-M-A49-031 and MOST 111-2811-M-A49-528.

Institutional Review Board Statement: Not applicable.

Informed Consent Statement: Not applicable.

Data Availability Statement: Not applicable.

Conflicts of Interest: The authors declare no conflict of interest.

References

1. Mitra, S.; Chakraborty, A.J.; Tareq, A.M.; Emran, T.B.; Nainu, F.; Khusro, A.; Idris, A.M.; Khandaker, M.U.; Osman, H.; Alhumaydhi, F.A.; et al. Impact of Heavy Metals on the Environment and Human Health: Novel Therapeutic Insights to Counter the Toxicity. *J. King Saud Univ. Sci.* **2022**, *34*, 101865. [CrossRef]
2. Gonçalves, A.R.P.; Paredes, X.; Cristino, A.F.; Santos, F.J.V.; Queirós, C.S.G.P. Ionic Liquids—A Review of Their Toxicity to Living Organisms. *Int. J. Mol. Sci.* **2021**, *22*, 5612. [CrossRef] [PubMed]
3. Hua, Y.; Ma, J.; Li, D.; Wang, R. DNA-Based Biosensors for the Biochemical Analysis: A Review. *Biosensors* **2022**, *12*, 183. [CrossRef] [PubMed]
4. Aktar, W.M.; Sengupta, D.; Chowdhury, A. Impact of Pesticides Use in Agriculture: Their Benefits and Hazards. *Interdisc Toxicol.* **2009**, *2*, 1–12. [CrossRef] [PubMed]
5. Gianessi, L.P. The Increasing Importance of Herbicides in Worldwide Crop Production. *Pest Manag. Sci.* **2013**, *69*, 1099–1105. [CrossRef]
6. Alberti, G.; Zanoni, C.; Magnaghi, L.R.; Biesuz, R. Gold and Silver Nanoparticle-Based Colorimetric Sensors: New Trends and Applications. *Chemosensors* **2021**, *9*, 305. [CrossRef]
7. Prosposito, P.; Burratti, L.; Venditti, I. Silver Nanoparticles as Colorimetric Sensors for Water Pollutants. *Chemosensors* **2020**, *8*, 26. [CrossRef]

8. Walekar, L.; Dutta, T.; Kumar, P.; Ok, Y.S.; Pawar, S.; Deep, A.; Kim, K.-H. Functionalized Fluorescent Nanomaterials for Sensing Pollutants in the Environment: A Critical Review. *TrAC Trends Anal. Chem.* **2017**, *97*, 458–467. [CrossRef]
9. Bulska, E.; Ruszczyńska, A. Analytical Techniques for Trace Element Determination. *Phys. Sci. Rev.* **2017**, *2*, 20178002.
10. Vervoort, N.; Goossens, K.; Baeten, M.; Chen, Q. Recent Advances in Analytical Techniques for High Throughput Experimentation. *Anal. Sci. Adv.* **2021**, *2*, 109–127. [CrossRef]
11. Kreno, L.E.; Leong, K.; Farha, O.K.; Allendorf, M.; Van Duyne, R.P.; Hupp, J.T. Metal–Organic Framework Materials as Chemical Sensors. *Chem. Rev.* **2012**, *112*, 1105–1125. [CrossRef]
12. Shellaiah, M.; Sun, K.-W. Progress in Metal-Organic Frameworks Facilitated Mercury Detection and Removal. *Chemosensors* **2021**, *9*, 101. [CrossRef]
13. Auwalu, M.A.; Cheng, S. Diketopyrrolopyrrole Fluorescent Probes, Photophysical and Biological Applications. *Chemosensors* **2021**, *9*, 44. [CrossRef]
14. Shellaiah, M.; Chen, Y.-T.; Thirumalaivasan, N.; Aazaad, B.; Awasthi, K.; Sun, K.W.; Wu, S.-P.; Lin, M.-C.; Ohta, N. Pyrene-Based AIEE Active Nanoprobe for Zn^{2+} and Tyrosine Detection Demonstrated by DFT, Bioimaging, and Organic Thin-Film Transistor. *ACS Appl. Mater. Interfaces* **2021**, *13*, 28610–28626. [CrossRef]
15. Cichosz, S.; Masek, A.; Zaborski, M. Polymer-Based Sensors: A Review. *Poly. Test.* **2018**, *67*, 342–348. [CrossRef]
16. Shellaiah, M.; Simon, T.; Thirumalaivasan, N.; Sun, K.W.; Ko, F.-H.; Wu, S.-P. Cysteamine-Capped Gold-Copper Nanoclusters for Fluorometric Determination and Imaging of Chromium(VI) and Dopamine. *Microchim. Acta* **2019**, *186*, 788. [CrossRef]
17. Terai, T.; Nagano, T. Fluorescent Probes for Bioimaging Applications. *Curr. Opin. Chem. Biol.* **2008**, *12*, 515–521. [CrossRef]
18. Sahoo, S.K.; Crisponi, G. Recent Advances on Iron(III) Selective Fluorescent Probes with Possible Applications in Bioimaging. *Molecules* **2019**, *24*, 3267. [CrossRef]
19. Shellaiah, M.; Awasthi, K.; Chandran, S.; Aazaad, B.; Sun, K.W.; Ohta, N.; Wu, S.-P.; Lin, M.-C. Methylammonium Tin Tribromide Quantum Dots for Heavy Metal Ion Detection and Cellular Imaging. *ACS Appl. Nano Mater.* **2022**, *5*, 2859–2874. [CrossRef]
20. Shellaiah, M.; Sun, K.-W. Pyrene-Based AIE Active Materials for Bioimaging and Theranostics Applications. *Biosensors* **2022**, *12*, 550. [CrossRef]
21. Chang, C.-C.; Chen, C.-P.; Wu, T.-H.; Yang, C.-H.; Lin, C.-W.; Chen, C.-Y. Gold Nanoparticle-Based Colorimetric Strategies for Chemical and Biological Sensing Applications. *Nanomaterials* **2019**, *9*, 861. [CrossRef] [PubMed]
22. Hussain, M.; Nafady, A.; Sirajuddin; Avcı, A.; Pehlivan, E.; Nisar, J.; Sherazi, S.T.H.; Balouch, A.; Shah, M.R.; Almaghrabi, O.A.; et al. Biogenic Silver Nanoparticles for Trace Colorimetric Sensing of Enzyme Disrupter Fungicide Vinclozolin. *Nanomaterials* **2019**, *9*, 1604. [CrossRef] [PubMed]
23. Shellaiah, M.; Simon, T.; Sun, K.W.; Ko, F.-H. Simple Bare Gold Nanoparticles for Rapid Colorimetric Detection of Cr^{3+} Ions in Aqueous Medium with Real Sample Applications. *Sens. Actuators B* **2016**, *226*, 44–51. [CrossRef]
24. Zhao, L.; Zhao, L.; Miao, Y.; Liu, C.; Zhang, C. A Colorimetric Sensor for the Highly Selective Detection of Sulfide and 1,4-Dithiothreitol Based on the In-Situ Formation of Silver Nanoparticles Using Dopamine. *Sensors* **2017**, *17*, 626. [CrossRef] [PubMed]
25. Dawadi, S.; Katuwal, S.; Gupta, A.; Lamichhane, U.; Thapa, R.; Jaisi, S.; Lamichhane, G.; Bhattarai, D.P.; Parajuli, N. Current Research on Silver Nanoparticles: Synthesis, Characterization, and Applications. *J. Nanomater.* **2021**, *2021*, 6687290. [CrossRef]
26. Shellaiah, M.; Simon, T.; Venkatesan, P.; Sun, K.W.; Ko, F.-H.; Wu, S.-P. Nanodiamonds Conjugated to Gold Nanoparticles for Colorimetric Detection of Clenbuterol and Chromium(III) in Urine. *Microchim. Acta* **2017**, *185*, 74. [CrossRef]
27. Sanskriti, I.; Upadhyay, K.K. Twinning as a Guiding Factor in Morphological Anisotropy of Silver Nanoparticles Stabilized Over L–DOPA: A Colorimetric Probe for Sulfide in Aqueous Medium. *ChemistrySelect* **2019**, *4*, 3803–3810. [CrossRef]
28. Shellaiah, M.; Thirumalaivasan, N.; Sun, K.W.; Wu, S.-P. A pH Cooperative Strategy for Enhanced Colorimetric Sensing of Cr(III) Ions Using Biocompatible L-Glutamic Acid Stabilized Gold Nanoparticles. *Microchem. J.* **2021**, *160*, 105754. [CrossRef]
29. Singh, R.; Mehra, R.; Walia, A.; Gupta, S.; Chawla, P.; Kumar, H.; Thakur, A.; Kaushik, R.; Kumar, N. Colorimetric Sensing Approaches Based on Silver Nanoparticles Aggregation for Determination of Toxic Metal Ions in Water Sample: A Review. *Inter. J. Environ. Anal. Chem.* **2021**, 1–16. [CrossRef]
30. Sabela, M.; Balme, S.; Bechelany, M.; Janot, J.-M.; Bisetty, K. A Review of Gold and Silver Nanoparticle-Based Colorimetric Sensing Assays. *Adv. Eng. Mater.* **2017**, *19*, 1700270. [CrossRef]
31. Guo, L.; Xu, Y.; Ferhan, A.R.; Chen, G.; Kim, D.-H. Oriented Gold Nanoparticle Aggregation for Colorimetric Sensors with Surprisingly High Analytical Figures of Merit. *J. Am. Chem. Soc.* **2013**, *135*, 12338–12345. [CrossRef]
32. Zhang, L.; Yuan, Y.; Wen, X.; Li, Y.; Cao, C.; Xiong, Q. A Coordination and Ligand Replacement Based Three-Input Colorimetric Logic Gate Sensing Platform for Melamine, Mercury Ions, and Cysteine. *RSC Adv.* **2015**, *5*, 59106–59113. [CrossRef]
33. Wang, N.; Yang, H.-F.; Zhu, X.; Zhang, R.; Wang, Y.; Huang, G.-F.; Zhang, Z.-R. Synthesis of Anti-aggregation Silver Nanoparticles Based on Inositol Hexakisphosphoric Micelles for A Stable Surface Enhanced Raman Scattering Substrate. *Nanotechnology* **2009**, *20*, 315603. [CrossRef]
34. Yang, L.; Wang, N.; Zheng, G. Enhanced Effect of Combining Chlorogenic Acid on Selenium Nanoparticles in Inhibiting Amyloid β Aggregation and Reactive Oxygen Species Formation In Vitro. *Nanoscale Res. Lett.* **2018**, *13*, 303. [CrossRef]
35. Yang, L.; Wang, W.; Chen, J.; Wang, N.; Zheng, G. A Comparative Study of Resveratrol and Resveratrol-Functional Selenium Nanoparticles: Inhibiting Amyloid β Aggregation and Reactive Oxygen Species Formation Properties. *J. Biomed. Mater. Res. A* **2018**, *106*, 3034–3041. [CrossRef]

36. Li, M.; Shi, P.; Xu, C.; Ren, J.; Qu, X. Cerium Oxide Caged Metal Chelator: Anti-aggregation and Anti-oxidation Integrated H_2O_2-responsive Controlled Drug Release for Potential Alzheimer's Disease Treatment. *Chem. Sci.* **2013**, *4*, 2536–2542. [CrossRef]
37. Ishtikhar, M.; Rahisuddin; Khan, M.V.; Khan, R.H. Anti-aggregation Property of Thymoquinone Induced by Copper-Nanoparticles: A Biophysical Approach. *Inter. J. Biol. Macromol.* **2016**, *93*, 1174–1182. [CrossRef]
38. Kong, L.; Zhou, X.; Shi, G.; Yu, Y. Molybdenum Disulfide Nanosheets-Based Fluorescent "Off-to-On" Probe for Targeted Monitoring and Inhibition of β-Amyloid Oligomers. *Analyst* **2020**, *145*, 6369–6377. [CrossRef]
39. Duangdeewong, C.; Choengchan, N.; Wattanasin, P.; Teerasong, S. Direct Determination of Ethanol in Alcoholic Beverages Based on Its Anti-aggregation of Melamine-Silver Nanoparticle Assembly. *Talanta* **2022**, *250*, 123751. [CrossRef]
40. Balali-Mood, M.; Naseri, K.; Tahergorabi, Z.; Khazdair, M.R.; Sadeghi, M. Toxic Mechanisms of Five Heavy Metals: Mercury, Lead, Chromium Cadmium, and Arsenic. *Front. Pharmacol.* **2021**, *12*, 643972. [CrossRef]
41. Lechuga, M.; Fernández-Serrano, M.; Jurado, E.; Núñez-Olea, J.; Ríos, F. Acute Toxicity of Anionic and Non-ionic Surfactants to Aquatic Organisms. *Ecotoxicol. Environ. Safety* **2016**, *125*, 1–8. [CrossRef] [PubMed]
42. Wang, T.; Ramnarayanan, A.; Cheng, H. Real Time Analysis of Bioanalytes in Healthcare, Food, Zoology and Botany. *Sensors* **2018**, *18*, 5. [CrossRef] [PubMed]
43. Dai, J.; Ma, C.; Zhang, P.; Fu, Y.; Shen, B. Recent Progress in the Development of Fuorescent Probes for Detection of Biothiols. *Dyes Pig.* **2020**, *177*, 108321. [CrossRef]
44. Defarge, N.; Spiroux de Vendômois, J.; Séralini, G.E. Toxicity of Formulants and Heavy Metals in Glyphosate-Based Herbicides and Other Pesticides. *Toxicol. Rep.* **2018**, *5*, 156–163. [CrossRef] [PubMed]
45. DeLorenzo, M.E.; Scott, G.I.; Ross, P.E. Toxicity of Pesticides to Aquatic Microorganisms: A Review. *Environ. Toxicol. Chem.* **2001**, *20*, 84–98. [CrossRef]
46. Najafzadeh, F.; Ghasemi, F.; Hormozi-Nezhad, M.R. Anti-aggregation of Gold Nanoparticles for Metal Ion Discrimination: A Promising Strategy to Design Colorimetric Sensor Arrays. *Sens. Actuators B* **2018**, *270*, 545–551. [CrossRef]
47. Li, Y.; Wu, P.; Xu, H.; Zhang, Z.; Zhong, X. Highly Selective and Sensitive Visualizable Detection of Hg^{2+} Based on Anti-aggregation of Gold Nanoparticles. *Talanta* **2011**, *84*, 508–512. [CrossRef]
48. Ding, N.; Zhao, H.; Peng, W.; He, Y.; Zhou, Y.; Yuan, L.; Zhang, Y. A Simple Colorimetric Sensor Based on Anti-aggregation of Gold Nanoparticles for Hg^{2+} Detection. *Colloids Surf. A* **2012**, *395*, 161–167. [CrossRef]
49. Lou, T.; Chen, L.; Zhang, C.; Kang, Q.; You, H.; Shen, D.; Chen, L. A Simple and Sensitive Colorimetric Method for Detection of Mercury Ions Based on Anti-aggregation of Gold Nanoparticles. *Anal. Methods* **2012**, *4*, 488–491. [CrossRef]
50. Li, Y.-L.; Leng, Y.-M.; Zhang, Y.-J.; Li, T.-H.; Shen, Z.-Y.; Wu, A.-G. A New Simple and Reliable Hg^{2+} Detection System Based on Anti-aggregation of Unmodified Gold Nanoparticles in the Presence of O-phenylenediamine. *Sens. Actuators B* **2014**, *200*, 140–146. [CrossRef]
51. Huang, G.G.; Chen, Y.-T.; Lin, Y.-R. Development of A Gold Nanoparticle Based Anti-aggregation Method for Rapid Detection of Mercury(ii) in Aqueous Solutions. *Anal. Methods* **2014**, *6*, 5690–5696. [CrossRef]
52. Zhou, Y.; Dong, H.; Liu, L.; Li, M.; Xiao, K.; Xu, M. Selective and Sensitive Colorimetric Sensor of Mercury (II) Based on Gold Nanoparticles and 4-Mercaptophenylboronic Acid. *Sens. Actuators B* **2014**, *196*, 106–111. [CrossRef]
53. Tang, J.; Wu, P.; Hou, X.; Xu, K. Modification-free and N-Acetyl-L-cysteine-Induced Colorimetric Response of AuNPs: A Mechanistic Study and Sensitive Hg^{2+} Detection. *Talanta* **2016**, *159*, 87–92. [CrossRef]
54. Jin, W.; Huang, P.; Wei, G.; Cao, Y.; Wu, F. Visualization and Quantification of Hg^{2+} Based on Anti-aggregation of Label-free Gold Nanoparticles in the Presence of 2-Mercaptobenzothiazole. *Sens. Actuators B* **2016**, *233*, 223–229. [CrossRef]
55. Rajeshwari, A.; Karthiga, D.; Chandrasekaran, N.; Mukherjee, A. Anti-aggregation-Based Spectrometric Detection of Hg(II) at Physiological pH Using Gold Nanorods. *Mater. Sci. Eng. C* **2016**, *67*, 711–716. [CrossRef]
56. Sun, X.; Liu, R.; Liu, Q.; Fei, Q.; Feng, G.; Shan, H.; Huan, Y. Colorimetric Sensing of Mercury (II) Ion Based on Anti-aggregation of Gold Nanoparticles in the Presence of Hexadecyl Trimethyl Ammonium Bromide. *Sens. Actuators B* **2018**, *260*, 998–1003. [CrossRef]
57. Kataria, R.; Sethuraman, K.; Vashisht, D.; Vashisht, A.; Mehta, S.K.; Gupta, A. Colorimetric Detection of Mercury Ions Based on Anti-aggregation of Gold Nanoparticles Using 3, 5-Dimethyl-1-thiocarboxamidepyrazole. *Microchem. J.* **2019**, *148*, 299–305. [CrossRef]
58. Mao, L.; Wang, Q.; Luo, Y.; Gao, Y. Detection of Ag^{+} Ions Via an Anti-aggregation Mechanism Using Unmodified Gold nanoparticles in the Presence of Thiamazole. *Talanta* **2021**, *222*, 121506. [CrossRef]
59. Selva Sharma, A.; SasiKumar, T.; Ilanchelian, M. A Rapid and Sensitive Colorimetric Sensor for Detection of Silver Ions Based on the Non-aggregation of Gold Nanoparticles in the Presence of Ascorbic Acid. *J. Cluster Sci.* **2018**, *29*, 655–662. [CrossRef]
60. Safavi, A.; Ahmadi, R.; Mohammadpour, Z. Colorimetric Sensing of Silver ion Based on Anti Aggregation of Gold Nanoparticles. *Sens. Actuators B* **2017**, *242*, 609–615. [CrossRef]
61. Gao, Q.; Zheng, Y.; Song, C.; Lu, L.-Q.; Tian, X.-K.; Xu, A.-W. Selective and Sensitive Colorimetric Detection of Copper Ions Based on Anti-aggregation of the Glutathione-Induced Aggregated Gold Nanoparticles and Its Application for Determining Sulfide Anions. *RSC Adv.* **2013**, *3*, 21424–21430. [CrossRef]
62. Hormozi-Nezhad, M.R.; Abbasi-Moayed, S. A Sensitive and Selective Colorimetric Method for Detection of Copper Ions Based on Anti-aggregation of Unmodified Gold Nanoparticles. *Talanta* **2014**, *129*, 227–232. [CrossRef] [PubMed]

63. Deng, H.-H.; Huang, K.-Y.; Fang, Q.-H.; Lv, Y.-P.; He, S.-B.; Peng, H.-P.; Xia, X.-H.; Chen, W. Schiff Base and Lewis Acid-Base Interaction-Regulated Aggregation/Dispersion of Gold Nanoparticles for Colorimetric Recognition of Rare-Earth Sc^{3+} Ions. *Sens. Actuators B* **2020**, *311*, 127925. [CrossRef]
64. Plaisen, S.; Cheewasedtham, W.; Rujiralai, T. Robust Colorimetric Detection Based on the Anti-aggregation of Gold Nanoparticles for Bromide in Rice Samples. *RSC Adv.* **2018**, *8*, 21566–21576. [CrossRef] [PubMed]
65. Chen, L.; Lu, W.; Wang, X.; Chen, L. A Highly Selective and Sensitive Colorimetric Sensor for Iodide Detection Based on Anti-aggregation of Gold Nanoparticles. *Sens. Actuators B* **2013**, *182*, 482–488. [CrossRef]
66. Zhou, G.; Zhao, C.; Pan, C.; Li, F. Highly Sensitive and Selective Colorimetric Detection of Iodide Based on Anti-Aggregation of Gold Nanoparticles. *Anal. Methods* **2013**, *5*, 2188–2192. [CrossRef]
67. Rasouli, Z.; Ghavami, R. Colorimetric Sensing of Iodide by the Competitive Interactions in the Surface of Gold Nanoparticles with the Simultaneous Aggregation/ Anti-Aggregation Mechanisms in Edible Salts. *Current Anal. Chem.* **2018**, *14*, 539–547. [CrossRef]
68. Peng, R.; He, H.; Wang, Q.; Yan, X.; Yu, Q.; Qin, H.; Lei, Y.; Luo, L.; Feng, Y. Cu(II) Triggering Redox-regulated Anti-aggregation of Gold Nanoparticles for Ultrasensitive Visual Sensing of Iodide. *Anal. Chim. Acta* **2018**, *1036*, 147–152. [CrossRef]
69. Pournaghi, A.; Keshvari, F.; Bahram, M. Colorimetric Determination of Iodine Based on Highly Selective and Sensitive Anti-aggregation Assay. *J. Iran. Chem. Soc.* **2019**, *16*, 143–149. [CrossRef]
70. Deng, H.-H.; Wu, C.-L.; Liu, A.-L.; Li, G.-W.; Chen, W.; Lin, X.-H. Colorimetric Sensor for Thiocyanate Based on Anti-aggregation of Citrate-Capped Gold Nanoparticles. *Sens. Actuators B* **2014**, *191*, 479–484. [CrossRef]
71. Song, J.; Huang, P.-C.; Wan, Y.-Q.; Wu, F.-Y. Colorimetric Detection of Thiocyanate Based on Anti-aggregation of Gold Nanoparticles in the Presence of Cetyltrimethyl Ammonium Bromide. *Sens. Actuators B* **2016**, *222*, 790–796. [CrossRef]
72. Zhao, Y.; Liu, R.; Cui, X.; Fu, Q.; Yu, M.; Fei, Q.; Feng, G.; Shan, H.; Huan, Y. Colorimetric Sensor for Thiocyanate Based on Anti-aggregation of Gold Nanoparticles in the Presence of 2-Aminopyridine. *Anal. Sci.* **2020**, *36*, 1165–1169. [CrossRef]
73. Lu, L.; Zhang, J.; Yang, X. Simple and Selective Colorimetric Detection of Hypochlorite Based on Anti-aggregation of Gold Nanoparticles. *Sens. Actuators B* **2013**, *184*, 189–195. [CrossRef]
74. Liu, W.; Du, Z.; Qian, Y.; Li, F. A Specific Colorimetric Probe for Phosphate Detection Based on Anti-aggregation of Gold Nanoparticles. *Sens. Actuators B* **2013**, *176*, 927–931. [CrossRef]
75. Ye, Y.; Guo, Y.; Yue, Y.; Zhang, Y. Facile Colorimetric Detection of Nitrite Based on Anti-Aggregation of Gold Nanoparticles. *Anal. Methods* **2015**, *7*, 4090–4096. [CrossRef]
76. Xu, H.; Wang, Y.; Huang, X.; Li, Y.; Zhang, H.; Zhong, X. Hg^{2+}-Mediated Aggregation of Gold Nanoparticles for Colorimetric Screening of Biothiols. *Analyst* **2012**, *137*, 924–931. [CrossRef]
77. Li, Z.-J.; Zheng, X.-J.; Zhang, L.; Liang, R.-P.; Li, Z.-M.; Qiu, J.-D. Label-Free Colorimetric Detection of Biothiols Utilizing SAM and Unmodified Au Nanoparticles. *Biosens. Bioelectron.* **2015**, *68*, 668–674. [CrossRef]
78. Li, Y.; Wu, P.; Xu, H.; Zhang, H.; Zhong, X. Anti-aggregation of Gold Nanoparticle-Based Colorimetric Sensor for Glutathione with Excellent Selectivity and Sensitivity. *Analyst* **2011**, *136*, 196–200. [CrossRef]
79. Li, J.-F.; Huang, P.-C.; Wu, F.-Y. Specific pH Effect for Selective Colorimetric Assay of Glutathione Using Anti-aggregation of Label-Free Gold Nanoparticles. *RSC Adv.* **2017**, *7*, 13426–13432. [CrossRef]
80. Li, J.-F.; Huang, P.-C.; Wu, F.-Y. Highly Selective and Sensitive Detection of Glutathione Based on Anti-aggregation of Gold Nanoparticles via pH Regulation. *Sens. Actuators B* **2017**, *240*, 553–559. [CrossRef]
81. Yuan, L.-F.; He, Y.-J.; Zhao, H.; Zhou, Y.; Gu, P. Colorimetric Detection of D-Amino Acids Based on Anti-aggregation of Gold Nanoparticles. *Chinese Chem. Lett.* **2014**, *25*, 995–1000. [CrossRef]
82. Huang, P.-C.; Gao, N.; Li, J.-F.; Wu, F.-Y. Colorimetric Detection of Methionine Based on Anti-aggregation of Gold Nanoparticles in the Presence of Melamine. *Sens. Actuators B* **2018**, *255*, 2779–2784. [CrossRef]
83. Keshvari, F.; Bahram, M.; Farhadi, K. A Selective, Sensitive and Label-Free Visual Assay of Fructose Using Anti-aggregation of Gold Nanoparticles as A Colorimetric Probe. *Chinese Chem. Lett.* **2016**, *27*, 847–851. [CrossRef]
84. Kim, H.-M.; Kim, W.-J.; Kim, K.-O.; Park, J.-H.; Lee, S.-K. Performance Improvement of A Glucose Sensor Based on Fiber Optic Localized Surface Plasmon Resonance and Anti-aggregation of the Non-Enzymatic Receptor. *J. Alloys Comp.* **2021**, *884*, 161140. [CrossRef]
85. Liu, S.; Du, Z.; Li, P.; Li, F. Sensitive Colorimetric Visualization of Dihydronicotinamide Adenine Dinucleotide Based on Anti-aggregation of Gold nanoparticles Via Boronic Acid–Diol Binding. *Biosens. Bioelectron.* **2012**, *35*, 443–446. [CrossRef]
86. Sang, F.; Zhang, X.; Liu, J.; Yin, S.; Zhang, Z. A Label-Free Hairpin Aptamer Probe for Colorimetric Detection of Adenosine Triphosphate Based on the Anti-aggregation of Gold Nanoparticles. *Spectrochim. Acta A* **2019**, *217*, 122–127. [CrossRef]
87. Zhang, Z.; Ye, X.; Liu, Q.; Hu, C.; Yun, J.; Liu, R.; Liu, Y. Colorimetric Nucleic Acid Detection Based on Gold Nanoparticles with Branched DNA. *Nano* **2020**, *15*, 2050110. [CrossRef]
88. Khurana, S.; Kukreti, S.; Kaushik, M. Designing A Two-Stage Colorimetric Sensing Strategy Based on Citrate Reduced Gold Nanoparticles: Sequential Detection of Sanguinarine (Anticancer Drug) and Visual Sensing of DNA. *Spectrochim. Acta A* **2021**, *246*, 119039. [CrossRef]
89. Zhang, C.; Liang, X.; You, T.; Yang, N.; Gao, Y.; Yin, P. An Ultrasensitive "Turn-Off" SERS Sensor for Quantitatively Detecting Heparin Based on 4-Mercaptobenzoic Acid Functionalized Gold Nanoparticles. *Anal. Methods* **2017**, *9*, 2517–2522. [CrossRef]
90. Ma, X.; Kou, X.; Xu, Y.; Yang, D.; Miao, P. Colorimetric Sensing Strategy for Heparin Assay Based on PDDA-Induced Aggregation of Gold Nanoparticles. *Nanoscale Adv.* **2019**, *1*, 486–489. [CrossRef]

91. Kim, H.Y.; Lee, D.; Ryu, K.-Y.; Choi, I. A Gold Nanoparticle-Mediated Rapid In Vitro Assay of Anti-aggregation Reagents for Amyloid β and Its Validation. *Chem. Commun.* **2017**, *53*, 4449–4452. [CrossRef]
92. Kim, H.Y.; Kwon, J.A.; Kang, T.; Choi, I. Rapid and High-Throughput Colorimetric Screening for Anti-aggregation Reagents of Protein Conformational Diseases by Using Gold Nanoplasmonic Particles. *Nanomed. Nanotechnol. Biol. Med.* **2017**, *13*, 1575–1585. [CrossRef]
93. Pasieka, A.; Panek, D.; Szałaj, N.; Espargaró, A.; Więckowska, A.; Malawska, B.; Sabaté, R.; Bajda, M. Dual Inhibitors of Amyloid-β and Tau Aggregation with Amyloid-β Disaggregating Properties: Extended In Cellulo, In Silico, and Kinetic Studies of Multifunctional Anti-Alzheimer's Agents. *ACS Chem. Neurosci.* **2021**, *12*, 2057–2068. [CrossRef]
94. Chang, C.-C.; Chen, C.-Y.; Chen, C.-P.; Lin, C.-W. Facile Colorimetric Detection of Human Chorionic Gonadotropin Based on the Peptide-Induced Aggregation of Gold Nanoparticles. *Anal. Methods* **2015**, *7*, 29–33. [CrossRef]
95. Wang, S.-T.; Lin, Y.; Spicer, C.D.; Stevens, M.M. Bio-Inspired Maillard-Like Reactions Enable A Simple and Sensitive Assay for Colorimetric Detection of Methylglyoxal. *Chem. Commun.* **2015**, *51*, 11026–11029. [CrossRef]
96. Su, R.; Xu, J.; Luo, Y.; Li, Y.; Liu, X.; Bie, J.; Sun, C. Highly Selective and Sensitive Visual Detection of Oxytetracycline Based on Aptamer Binding-Mediated the Anti-Aggregation of Positively Charged Gold Nanoparticles. *Mater. Lett.* **2016**, *180*, 31–34. [CrossRef]
97. Chen, Z.; Chen, L.; Lin, L.; Wu, Y.; Fu, F. A Colorimetric Sensor for the Visual Detection of Azodicarbonamide in Flour Based on Azodicarbonamide-Induced Anti-Aggregation of Gold Nanoparticles. *ACS Sens.* **2018**, *3*, 2145–2151. [CrossRef]
98. Liu, G.; Zhang, R.; Li, L.; Huang, X.; Li, T.; Lu, M.; Xu, D.; Wang, J. Anti-Agglomeration Behavior and Sensing Assay of Chlorsulfuron Based on Acetamiprid-Gold Nanoparticles. *Nanomaterials* **2018**, *8*, 499. [CrossRef]
99. Liu, G.; Zhang, R.; Huang, X.; Li, L.; Liu, N.; Wang, J.; Xu, D. Visual and Colorimetric Sensing of Metsulfuron-Methyl by Exploiting Hydrogen Bond-Induced Anti-Aggregation of Gold Nanoparticles in the Presence of Melamine. *Sensors* **2018**, *18*, 1595. [CrossRef]
100. Keshvari, F.; Bahram, M. Selective, Sensitive and Reliable Colorimetric Sensor for Catechol Detection Based on Anti-aggregation of Unmodified Gold Nanoparticles Utilizing Boronic Acid–Diol Reaction: Optimization by Experimental Design Methodology. *J. Iran. Chem. Soc.* **2017**, *14*, 977–984. [CrossRef]
101. Chen, N.; Liu, H.; Zhang, Y.; Zhou, Z.; Fan, W.; Yu, G.; Shen, Z.; Wu, A. A Colorimetric Sensor Based on Citrate-Stabilized AuNPs for Rapid Pesticide Residue Detection of Terbuthylazine and Dimethoate. *Sens. Actuators B* **2018**, *255*, 3093–3101. [CrossRef]
102. Li, D.; Wang, S.; Wang, L.; Zhang, H.; Hu, J. A Simple Colorimetric Probe Based on Anti-aggregation of AuNPs for Rapid and Sensitive Detection of Malathion in Environmental Samples. *Anal. Bioanal. Chem.* **2019**, *411*, 2645–2652. [CrossRef] [PubMed]
103. Chungchai, W.; Amatatongchai, M.; Meelapsom, R.; Seebunrueng, K.; Suparsorn, S.; Jarujamrus, P. Development of A Novel Three-Dimensional Microfluidic Paper-Based Analytical Device (3D-μPAD) for Chlorpyrifos Detection Using Graphene Quantum-dot Capped Gold Nanocomposite for Colorimetric Assay. *Inter. J. Environ. Anal. Chem.* **2020**, *100*, 1160–1178. [CrossRef]
104. Liu, K.; Jin, Y.; Wu, Y.; Liang, J. Simple and Rapid Colorimetric Visualization of Tetramethylthiuram Disulfide (Thiram) Sensing Based on Anti-aggregation of Gold Nanoparticles. *Food Chem.* **2022**, *384*, 132223. [CrossRef] [PubMed]
105. Zhou, Z.; Zhang, Y.; Kang, J.; Dong, C.; Chen, N.; Li, X.; Guo, Z.; Wu, A. Detection of Herbicide Glyphosates Based on An Anti-aggregation Mechanism by Using Unmodified Gold Nanoparticles in the Presence of Pb^{2+}. *Anal. Methods* **2017**, *9*, 2890–2896. [CrossRef]
106. Duan, J.; Yin, H.; Wei, R.; Wang, W. Facile Colorimetric Detection of Hg^{2+} Based on Anti-aggregation of Silver Nanoparticles. *Biosens. Bioelectron.* **2014**, *57*, 139–142. [CrossRef]
107. Ye, Y.; Guo, Y.; Yue, Y.; Huang, H.; Zhao, L.; Gao, Y.; Zhang, Y. Colorimetric Sensing of Copper Ions Based on the Anti-aggregation of Unmodified Silver Nanoparticles in the Presence of 1,4-Dithiothreitol. *Anal. Methods* **2015**, *7*, 566–572. [CrossRef]
108. He, Y.; Zhang, X. Ultrasensitive Colorimetric Detection of Manganese(II) Ions Based on Anti-aggregation of Unmodified Silver Nanoparticles. *Sens. Actuators B* **2016**, *222*, 320–324. [CrossRef]
109. Basiri, S.; Mehdinia, A.; Jabbari, A. Green Synthesis of Reduced Graphene Oxide-Ag Nanoparticles as A Dual-Responsive Colorimetric Platform for Detection of Dopamine and Cu^{2+}. *Sens. Actuators B* **2018**, *262*, 499–507. [CrossRef]
110. Bothra, S.; Kumar, R.; Pati, R.K.; Kuwar, A.; Choi, H.-J.; Sahoo, S.K. Virgin Silver Nanoparticles as Colorimetric Nanoprobe for Simultaneous Detection of Iodide and Bromide Ion in Aqueous Medium. *Spectrochim. Acta A* **2015**, *149*, 122–126. [CrossRef]
111. Motahhari, A.; Abdolmohammad-Zadeh, H.; Farhadi, K. Development of A New Fluoride Colorimetric Sensor Based on Anti-aggregation of Modified Silver Nanoparticles. *Anal. Bioanal. Chem. Res.* **2021**, *8*, 79–89.
112. Dong, C.; Ma, X.; Qiu, N.; Zhang, Y.; Wu, A. An Ultra-Sensitive Colorimetric Sensor Based on Smartphone for Pyrophosphate Determination. *Sens. Actuators B* **2021**, *329*, 129066. [CrossRef]
113. Pinyorospathum, C.; Rattanarat, P.; Chaiyo, S.; Siangproh, W.; Chailapakul, O. Colorimetric Sensor for Determination of Phosphate Ions Using Anti-aggregation of 2-Mercaptoethanesulfonate-Modified Silver Nanoplates and Europium Ions. *Sens. Actuators B* **2019**, *290*, 226–232. [CrossRef]
114. Chen, L.; Fu, X.; Li, J. Ultrasensitive Surface-Enhanced Raman Scattering Detection of Trypsin Based on Anti-aggregation of 4-Mercaptopyridine-Functionalized Silver Nnanoparticles: An Optical Sensing Platform Toward Proteases. *Nanoscale* **2013**, *5*, 5905–5911. [CrossRef]

115. Trisaranakul, W.; Chompoosor, A.; Maneeprakorn, W.; Nacapricha, D.; Choengchan, N.; Teerasong, S. A Simple and Rapid Method Based on Anti-aggregation of Silver Nanoparticles for Detection of Poly(diallyldimethylammonium chloride) in Tap Water. *Anal. Sci.* **2016**, *32*, 769–773. [CrossRef]
116. Shellaiah, M.; Sun, K.W. Review on Nanomaterial-Based Melamine Detection. *Chemosensors* **2019**, *7*, 9. [CrossRef]
117. Abdel-Lateef, M.A.; Almahri, A.; Alzahrani, E.; Pashameah, R.A.; Abu-Hassan, A.A.; El Hamd, M.A. Sustainable PVP-Capped Silver Nanoparticles as a Free-Standing Nanozyme Sensor for Visual and Spectrophotometric Detection of Hg^{2+} in Water Samples: A Green Analytical Method. *Chemosensors* **2022**, *10*, 358. [CrossRef]
118. Mochi, F.; Burratti, L.; Fratoddi, I.; Venditti, I.; Battocchio, C.; Carlini, L.; Iucci, G.; Casalboni, M.; De Matteis, F.; Casciardi, S.; et al. Plasmonic Sensor Based on Interaction between Silver Nanoparticles and Ni^{2+} or Co^{2+} in Water. *Nanomaterials* **2018**, *8*, 488. [CrossRef]
119. Rossi, A.; Zannotti, M.; Cuccioloni, M.; Minicucci, M.; Petetta, L.; Angeletti, M.; Giovannetti, R. Silver Nanoparticle-Based Sensor for the Selective Detection of Nickel Ions. *Nanomaterials* **2021**, *11*, 1733. [CrossRef]
120. Liu, X.; Wang, J.; Wang, Y.; Huang, C.; Wang, Z.; Liu, L. In Situ Functionalization of Silver Nanoparticles by Gallic Acid as a Colorimetric Sensor for Simple Sensitive Determination of Melamine in Milk. *ACS Omega* **2021**, *6*, 23630–23635. [CrossRef]
121. Sharma, R.; Dhillon, A.; Kumar, D. Mentha-Stabilized Silver Nanoparticles for High-Performance Colorimetric Detection of Al(III) in Aqueous Systems. *Sci. Rep.* **2018**, *8*, 5189. [CrossRef] [PubMed]
122. Omar, N.A.S.; Fen, Y.W.; Irmawati, R.; Hashim, H.S.; Ramdzan, N.S.M.; Fauzi, N.I.M. A Review on Carbon Dots: Synthesis, Characterization and Its Application in Optical Sensor for Environmental Monitoring. *Nanomaterials* **2022**, *12*, 2365. [CrossRef] [PubMed]
123. Shellaiah, M.; Sun, K.W. Review on Sensing Applications of Perovskite Nanomaterials. *Chemosensors* **2020**, *8*, 55. [CrossRef]
124. Anas, N.A.A.; Fen, Y.W.; Omar, N.A.S.; Daniyal, W.M.E.M.M.; Ramdzan, N.S.M.; Saleviter, S. Development of Graphene Quantum Dots-Based Optical Sensor for Toxic Metal Ion Detection. *Sensors* **2019**, *19*, 3850. [CrossRef] [PubMed]
125. Shellaiah, M.; Sun, K.W. Luminescent Metal Nanoclusters for Potential Chemosensor Applications. *Chemosensors* **2017**, *5*, 36. [CrossRef]
126. Shellaiah, M.; Thirumalaivasan, N.; Aazaad, B.; Awasthi, K.; Sun, K.W.; Wu, S.-P.; Lin, M.-C.; Ohta, N. An AIEE Active Anthracene-Based Nanoprobe for Zn^{2+} and Tyrosine Detection Validated by Bioimaging Studies. *Chemosensors* **2022**, *10*, 381. [CrossRef]
127. Shellaiah, M.; Simon, T.; Srinivasadesikan, V.; Lin, C.-M.; Sun, K.W.; Ko, F.-H.; Lin, M.-C.; Lin, H.-C. Novel Pyrene Containing Monomeric and Dimeric Supramolecular AIEE Active Nano-Probes Utilized in Sselective "Off–On" Trivalent Metal and Highly Acidic pH Sensing with Live Cell Applications. *J. Mater. Chem. C* **2016**, *4*, 2056–2071. [CrossRef]
128. Olean-Oliveira, A.; Oliveira Brito, G.A.; Cardoso, C.X.; Teixeira, M.F.S. Nanocomposite Materials Based on Electrochemically Synthesized Graphene Polymers: Molecular Architecture Strategies for Sensor Applications. *Chemosensors* **2021**, *9*, 149. [CrossRef]
129. Shellaiah, M.; Simon, T.; Venkatesan, P.; Sun, K.W.; Ko, F.-H.; Wu, S.-P. Cysteamine-Modified Diamond Nanoparticles Applied in Cellular Imaging and Hg^{2+} Ions Detection. *Appl. Surf. Sci.* **2019**, *465*, 340–350. [CrossRef]
130. Shellaiah, M.; Sun, K.W. Conjugation of cysteamine functionalized nanodiamond to gold nanoparticles for pH enhanced colorimetric detection of Cr^{3+} ions demonstrated by real water sample analysis. *Spectrochim. Acta A* **2022**, *286*, 121962. [CrossRef]
131. Nguyen, V.-N.; Ha, J.; Cho, M.; Li, H.; Swamy, K.M.K.; Yoon, J. Recent Developments of BODIPY-Based Colorimetric and Fluorescent Probes for the Detection of Reactive Oxygen/Nitrogen Species and Cancer diagnosis. *Coord. Chem. Rev.* **2021**, *439*, 213936. [CrossRef]
132. Arumugaperumal, R.; Srinivasadesikan, V.; Lin, M.-C.; Shellaiah, M.; Shukla, T.; Lin, H.-C. Facile Rhodamine-Based Colorimetric Sensors for Sequential Detections of Cu(ii) Ions and Pyrophosphate ($P_2O_7^{4-}$) Anions. *RSC Adv.* **2016**, *6*, 106631–106640. [CrossRef]
133. Liu, B.; Zhuang, J.; Wei, G. Recent Advances in the Design of Colorimetric Sensors for Environmental Monitoring. *Environ. Sci. Nano* **2020**, *7*, 2195–2213. [CrossRef]
134. Fang, H.-P.; Shellaiah, M.; Singh, A.; Raju, M.V.R.; Wu, Y.-H.; Lin, H.-C. Naked Eye and Fluorescent Detections of Hg^{2+} Ions and Cysteine via *J*-Aggregation and Deaggregation of a Perylene Bisimide Derivative. *Sens. Actuators B* **2014**, *194*, 229–237. [CrossRef]
135. Shellaiah, M.; Thirumalaivasan, N.; Aazaad, B.; Awasthi, K.; Sun, K.W.; Wu, S.-P.; Lin, M.-C.; Ohta, N. Novel Rhodamine Probe for Colorimetric and Fluorescent Detection of Fe^{3+} Ions in Aqueous Media with Cellular Imaging. *Spectrochim. Acta A* **2020**, *242*, 118757. [CrossRef]
136. Chen, S.; Xue, Z.; Gao, N.; Yang, X.; Zang, L. Perylene Diimide-Based Fluorescent and Colorimetric Sensors for Environmental Detection. *Sensors* **2020**, *20*, 917. [CrossRef]
137. Ericson, M.N.; Shankar, S.K.; Chahine, L.M.; Omary, M.A.; Herbing, I.H.v.; Marpu, S.B. Development of Neutral Red as a pH/pCO_2 Luminescent Sensor for Biological Systems. *Chemosensors* **2021**, *9*, 210. [CrossRef]